2019-01-01

A Modified Wilshire Model For Creep Deformation And Damage Prediction

Jaime Aaron Cano
University of Texas at El Paso

A MODIFIED WILSHIRE MODEL FOR CREEP DEFORMATION AND DAMAGE PREDICTION

JAIME AARON CANO ESCAMILLA

Master's Program in Mechanical Engineering

APPROVED:

Calvin M. Stewart, Ph.D., Chair

Yirong Lin, Ph.D.

Cesar Carrasco, Ph.D.

Stephen L. Crites, Ph.D.
Dean of the Graduate School

DEDICATION

Dedicated to God

“Ad maiorem Dei gloriam”

A MODIFIED WILSHIRE MODEL FOR CREEP DEFORMATION AND DAMAGE PREDICTION

by

JAIME AARON CANO ESCAMILLA, B.Sc.

THESIS

Presented to the Faculty of the Graduate School of

The University of Texas at El Paso

in Partial Fulfillment

of the Requirements

for the Degree of

MASTER OF SCIENCE

Department of Mechanical Engineering

THE UNIVERSITY OF TEXAS AT EL PASO

December 2019

ACKNOWLEDGMENTS

I would like to thank Dr. Calvin M. Stewart for his guidance and mentorship through this journey. I would like to thank my family and especially my mother Irma Escamilla for being my support and example in pursuing a higher level of education. I would also like to thank my community and close friends as they encourage me to become better by recognizing the needs on the world. Lastly, I would like to thank the Department of Energy (DOE) National Energy Technology Laboratory for funding my research under Award Number(s) DE-FE0027581.

ABSTRACT

In this work, a new constitutive model, the WCS model, is derived that combines the Wilshire equations with continuum damage mechanics (CDM) for the long-term prediction of creep deformation, damage, and rupture. Long-term creep data is expensive and time-consuming to obtain because conventional creep testing is real-time. There is a need to extrapolate long-term creep behaviors from short-term data. Models that can accurately predict long-term creep behavior over a wide range of boundary conditions are vital for design engineers. The classic Wilshire equations can accurately extrapolate the long-term stress-rupture, minimum-creep-strain-rate, and time-to-strain of various alloys as their functional form has an explicit description of stress and temperature dependency. Recently, the time-to-creep-strain equation has been exploited to generate full creep deformation curves; however, with the addition of a CDM model, the equations become suitable for finite element analysis (FEA). The Sinh model can predict creep deformation, damage, and has been implemented into FEA software; however it lacks a description of temperature-dependence which limits the range in which predictions can be made. The combination of the Wilshire and the Sinh model enables stress-rupture, minimum-creep-strain-rate, creep deformation, and damage predictions with explicit stress and temperature dependency. In order to accomplish this goal; **(a)** the current Wilshire equations are evaluated for one material in in different forms and **(b)** the new CDM-based WCS model is developed and the realistic performance of the model is assessed. The WCS model predicts creep behaviors such as stress-rupture, minimum-creep-strain-rate, damage evolution, and creep deformation with an explicit stress and temperature gradients. The explicitness of the stress and temperature gradients across makes the model suitable for FEA software. Parametric studies are performed on the WCS model and is observed that the model behaves in a realistic manner.

TABLE OF CONTENTS

LIST OF TABLES

LIST OF FIGURES

CHAPTER 1: INTRODUCTION

1.1 Motivation

Drives to increase the efficiency of Advance Ultrasupercritical (A-USC) and Fossil Energy (FE) power plants lead to designs with steam pressures up to 4000 psi and temperatures ranging $0.3T_m < T < 0.6T_m$, where T_m is the melting temperature of the specific material. The complexity in which these power plants operate, especially for the hot gas path in industrial gas turbines (IGTs) illustrated in Figure 1.1, pushes the limits of material science and the properties of materials [1]. Failure that occurs on IGTs turbine blades are caused by many phenomena such as fatigue and creep which are encounter at the extreme conditions that power plants operate [2-3]. Maintenance must be performed regularly to avoid catastrophic failure, as illustrated in the turbine blade of Figure 1.2, caused by creep and combined damage factors [4]. Maintenance costs are of the major concern in IGTs which inspections of hot gas path components occurring every 2 years and major inspections between 4 and 5 years [5]. Unexpected failures can emerge in the time interval in which inspections are made, due to the uncertainty and the continuum damage that creep generates. There is a need to predict these behaviors accurately to have a better maintenance interval and to avoid failures.

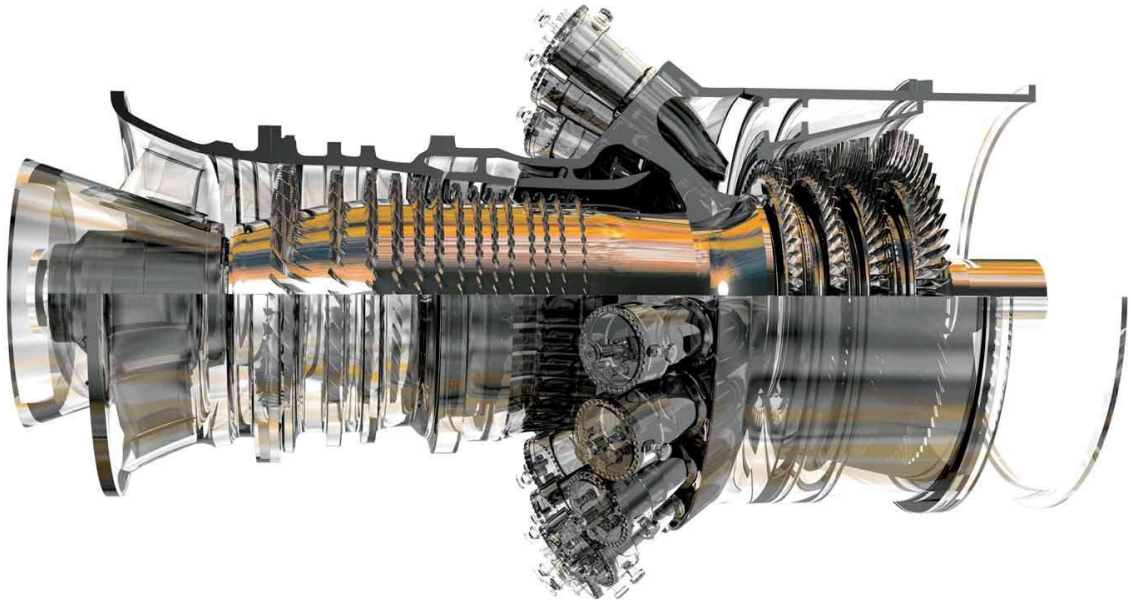

Figure 1.1 – GE H-Class 9HA.01/.02 Gas Turbine (50 Hz) (9HA.01 at 446 MW and the 9HA.02 at 571 MW) [5].

Figure 1.2 – Industrial gas turbine blade creep failure (Berkeley Research Company, Berkeley California) [4].

The current understanding and ability to predict long-term creep behaviors ($\geq 10^5$ hours) such as rupture time, minimum-creep-strain-rate (MCSR) and creep deformation curves, and damage is limited. Long-term creep is difficult to predict due to the lack of data at such extreme durations; where experiments must run continuously for greater than 10 years [6]. Over the years, an immense number of models have been developed as an alternative of conducting those long duration experiments. Numerous constitutive models have been developed to predict the creep deformation of materials; however extrapolations are not as accurate for some models and for others is impossible because of the complex dependence on stress and its parameters [6-8]. There is a need for reliable prediction methods with stress and temperature dependency to better extrapolate creep and damage behavior and to perform finite element simulations as well.

1.2 Research Objectives

The objective of this research study is to develop a continuum damage model (CDM) using the Wilshire equations, the WCS model, that can predict long-term creep deformation, damage, and rupture with explicit stress and temperature dependency. The goals are to **(a)** assess the current Wilshire laws, and **(b)** developed the novel CDM WCS model and validate the realistic performance of the model. To accomplish goal

(a) the Wilshire stress-rupture and minimum-creep-strain-rate (MCSR) equations predictive capabilities are assessed using short-term data ($<10^4$). The equations are calibrated to alloy P91 data in tube, plate and pipe form. Post-audit validation is performed using long-term data ($\geq 10^4$) and the normalized-mean-squared error (NMSE) is reported for each material isotherm and material form. Additionally, using the stress-rupture equation, contour design maps are created as tools for design engineers.

(b) the new WCS model is derived, where the Wilshire stress-rupture and MCSR equations are incorporated into the Sinh CDM model. Creep deformation data is collected for alloy P91 for a single isotherm and multiple stress levels and is fitted to the model. Material constants are obtained for the WCS model using the calibration approach from the Wilshire equations and the Sinh model. Using the material constants, plots for creep deformation and damage demonstrate the accuracy of the novel model. A parametric study is performed to assess the interpolation and extrapolation ability of the novel model.

1.3 Organization

The organization of this study is as follows: Chapter 2 provides background information on creep deformation and damage. Some constitutive models that have predicted different creep behaviors, such as MCSR and creep deformation, are discussed in a non-exhaustive manner. Chapter 3 introduces and describes the material used in each study providing mechanical properties and nominal chemical composition. Data is introduced in Chapter 3 and used in Chapter 4 for the application of the Wilshire equations, stress-rupture and MCSR, using alloy P91 tube, plate, and pipe form. The Wilshire equations are introduced in this chapter as well as the calibration approach. The model is then fitted, and post-audit validation is performed to vet the accuracy of the models. Chapter 5 introduces the novel WCS model for creep deformation and damage predictions. Material constants are obtained, and the model is calibrated to generate predictions. After the model is calibrated to the data, parametric simulations are performed to vet the performance of the model in realistic scenarios. Finally, Chapter 6 offers an overview of the results and conclusions as well as the future work that is related to this area of study.

CHAPTER 2: BACKGROUND

2.1 Introduction

In order to create the novel WCS model, background study is needed to understand creep phenomenon. Creep is a phenomenological event that is divided in regimes. Many models are designed to understand different behaviors such as rupture time, MCSR, and creep deformation. A brief summary of a few traditional models is provided as well as their current limitations. Understanding such limitations provides guidelines on recent modeling needs and how the WCS model addresses such issues. Note both the Wilshire model and CDM Sinh model are not included on this analysis as they are discussed later to give a stronger flow to the narrative.

2.2 Creep Phenomenon

Creep is a rate-dependent non-recoverable plastic deformation of materials as a function of stress and temperature [9]. The resulting conventional creep deformation curve is illustrated in Figure 2.1 [9]. Creep strain is activated thermally, and when stress is applied, typically to a metal or ionic solid, deformation leading to failure arises [10]. Most high temperature failures in materials are attribute to creep, fatigue, and combinations of damage [11]. Temperature ranges for creep deformation are: $T > 0.6T_m$ for high temperature , where T_m is the melting temperature, $0.3T_m < T < 0.6T_m$ for intermediate temperatures and $T < 0.3T_m$ for low temperature [2]. Assuming constant stress, high and intermediate temperatures generate short rupture times and low temperatures might extend to infinite life. There is an interest in such low temperature studies as many models intend to predict decades of life. Mechanical systems such as gas turbines, nuclear reactors, and chemical industries operate at these temperature ranges [11]. Therefore creep is

dependent on high temperatures as well as mixed conditions such as applied stress, geometry, and time.

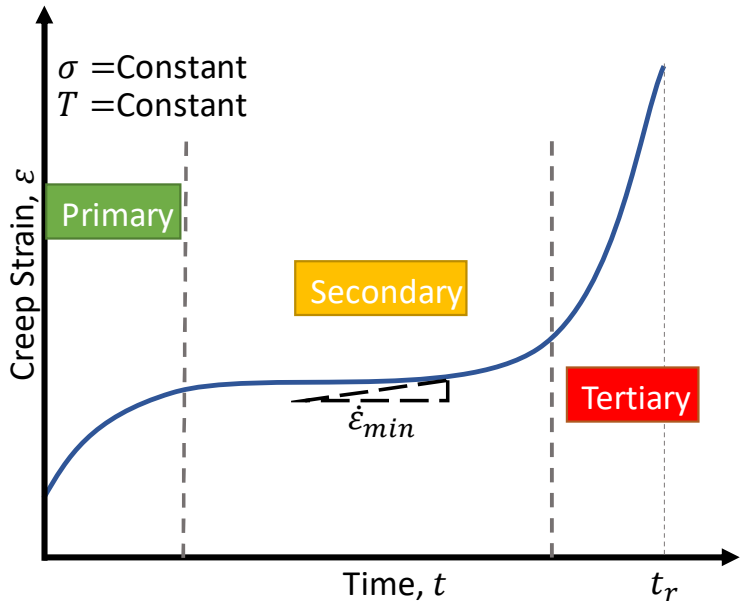

Figure 2.1 – Idealized conventional creep deformation curve [9].

In 1910, Andrade divided the creep deformation curve into three stages or regimes [12]. Those regimes are: the primary regime also called transient creep, the secondary regime called steady-state creep, and the tertiary regime called the accelerating creep, where rupture comes in the tertiary regime as shown in Figure 2.1 [9-13]. Depending on the material the arrangement of these creep regimes might vary. Many materials lack a primary regime or at high stress and temperatures exhibit only a short (transitional) secondary regime. Some brittle materials have little to no tertiary creep while ductile materials would have an extensive tertiary creep regime [10-11]. Some materials have an instantaneous response called ε_0 that depends on the magnitude of the applied stress, this instantaneous response is most of the primary creep regime [9]. Other materials have microstructural mechanism such as precipitate carbides that prevents grain boundary sliding.

Such materials exhibit little primary creep which, in many models, is typically neglected. Primary creep normally reaches its peak in a short time which contributes in the case of neglecting it in modeling. The secondary regime is large and has similar characteristics as plastic deformations [13]. Most mathematical models use this dominant steady-state behavior to approximate the creep curve. Such behavior is called the minimum-creep-strain-rate, $\dot{\varepsilon}_{\min}$ which as shown in Figure 2.1 is almost constant [9]. In the tertiary regime failure happens at a rapid rate and arrives as an unexpected behavior most of the time. Grain boundary sliding contributes to crack propagation and void nucleation and growth which ultimately leads to rupture of a specimen [11].

The dependency of creep from stress and temperature, strongly impacts the creep deformation curves. The influenced in stress where temperature is constant is observed in Figure 2.2 a). Notice that as stress increases creep ductility is achieved at a faster time. Similarly, the temperature dependency at constant stress portraits a similar behavior as shown in Figure 2.2 b). It is observed that when the temperature is constant and different stress levels are applied ($\sigma_3 > \sigma_2 > \sigma_1$) then the rupture time has dramatic impact that can range even for decades of life. Similarly, when stress is constant and distinct isotherms are applied ($T_3 > T_2 > T_1$). Additionally, each individual curve generated has a corresponding $\dot{\varepsilon}_{\min}$ where some creep curves can even transition from the primary to the tertiary regime at high levels of stress and temperature [9,11].

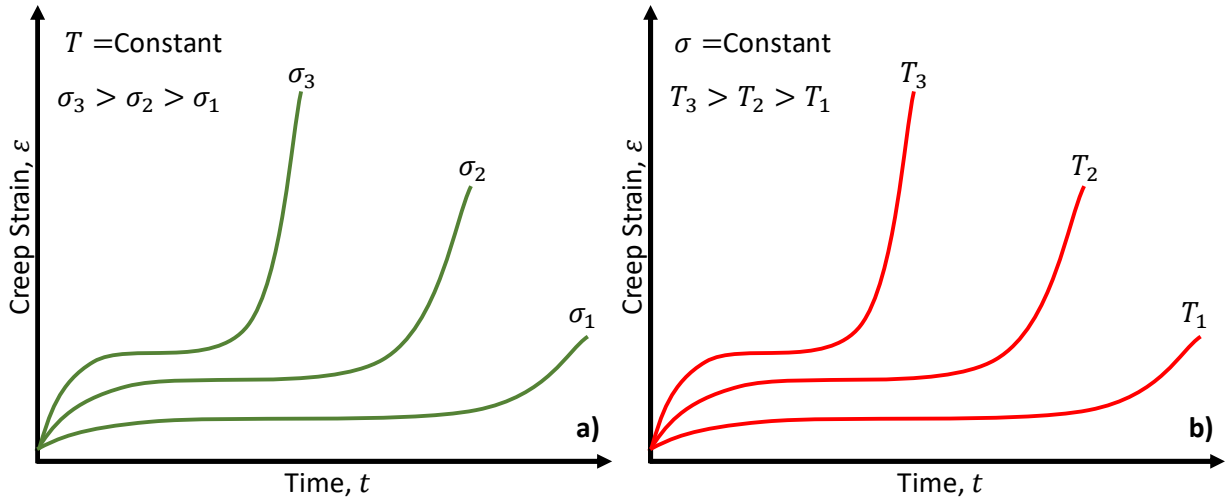

Figure 2.2 – Idealized creep deformation curves as a function of a) stress at constant temperature and b) temperature at constant stress. [9,11]

2.3 Constitutive Models and Creep Modeling

Creep constitutive models are considered a viscoplasticity models, where viscoplastic materials sustain a shear stress at rest [13,14]. Typically constitutive creep models are either microstructural or phenomenological. Microstructural models are based on the creep deformation behaviors within the microstructure such as the nucleation of cavities within the grain boundaries. This study focuses more on phenomenological models. The phenomenological models are based on the material properties representing the response of the continua. The calibration process to obtain material constants for phenomenological models is either analytical, numerical, or a combination of both methods.

Creep mechanisms create functional relations that are the base theory for many existing constitutive models. According to Frost and Ashby polycrystalline solids yield strength and material properties of materials are define by the processes occurring at the atomic scale [15].

Mechanisms which describe such atomic processes are therefore called deformation mechanisms. There are mainly five groups of deformation mechanisms

- *Collapse at ideal yield strength.* After exceeding a shear strength flow occurs.
- *Low-temperature plasticity by dislocation glide.* Limited by the lattice resistance, discrete obstacles, phonon, drags, and influenced by adiabatic heating.
- *Low-temperature plasticity by twinning.* Dislocation glides involving partial dislocation motions.
- *Power-law creep by dislocation glide.* Limited by glide processes, lattice-diffusion controlled climb, corediffusion controlled climb, power-law breakdown, Harper-Dorn creep, and creep with dynamic recrystallization.
- *Diffusional flow.* Limited by Nabarro-Herring lattice-diffusion creep or bulk diffusion, coble creep or grain boundary diffusion, and interface-reaction controlled diffusion flow.

This deformation mechanisms are presented in deformation mechanisms maps. The constitutive laws for such mechanisms maps are describe in the following rate equations

$$\dot{\varepsilon} = f\left(\sigma_s, T, S_i, P_i\right) \tag{2.1}$$

$$\frac{dS_i}{dt} = g\left(\sigma_s, T, S_i, P_i\right) \tag{2.2}$$

where the shear strain-rate $\dot{\varepsilon}$ is a function of the shearing or deviatoric stress field σ_s, the temperature T, the state variables S_i, and the material plastic properties P_i. The shearing or deviatoric stress field is defined as

$$\sigma_s = \sqrt{\frac{1}{6}\left(\left(\sigma_1 - \sigma_2\right)^2 + \left(\sigma_2 + \sigma_3\right)^2 + \left(\sigma_3 + \sigma_1\right)^2\right)} \tag{2.3}$$

where σ_1, σ_2, and σ_3 are the principal stresses. Both [Eq. (2.1)] and [Eq. (2.2)] can be integrated with respect to time. The current understanding of the evolution of the structure is limited therefore typically S_i is assumed as a constant structure or at steady state. In order to simplify the rate equation the assumptions are used in [Eq. (2.2)] to obtained S_1, S_2, and S_3 in terms of σ_s and T leading to a single equation in the following form

$$\dot{\varepsilon} = f\left(\sigma_s, T\right) \tag{2.4}$$

where properties for P_i are constant. It is useful to create deformation mechanism maps to make better prediction of creep at distinct isotherms and stress levels. A typical schematic illustration of a deformation mechanism is given in Figure 2.3 [15-16]. The schematic is given as a plot of the normalized equivalent stress σ_{eq}/G with respect to the shear modulus versus the homologous temperature T/T_m where T_m is the melting temperature. It is shown that over a wide range of stress and temperature distinct mechanism are considered. Every combination of the stress and temperature results in a contour representation of the mechanism and their respective strain rate, $\dot{\varepsilon}$. Another example of creep deformation mechanism map is given for alloy 9Cr-1Mo-V-Nb (P91) steel illustrated in Figure 2.4 [16]. It can be observed that in order to properly model for alloy P91 both mechanisms of power-law and linear/viscous creep must be taken into consideration.

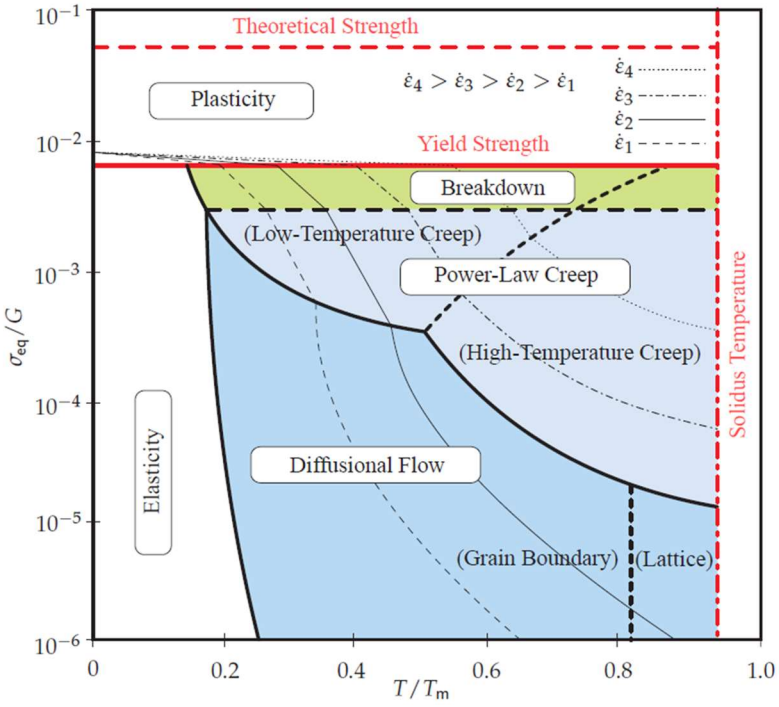

Figure 2.3 – Schematic illustration of a typical deformation mechanism map [15-16].

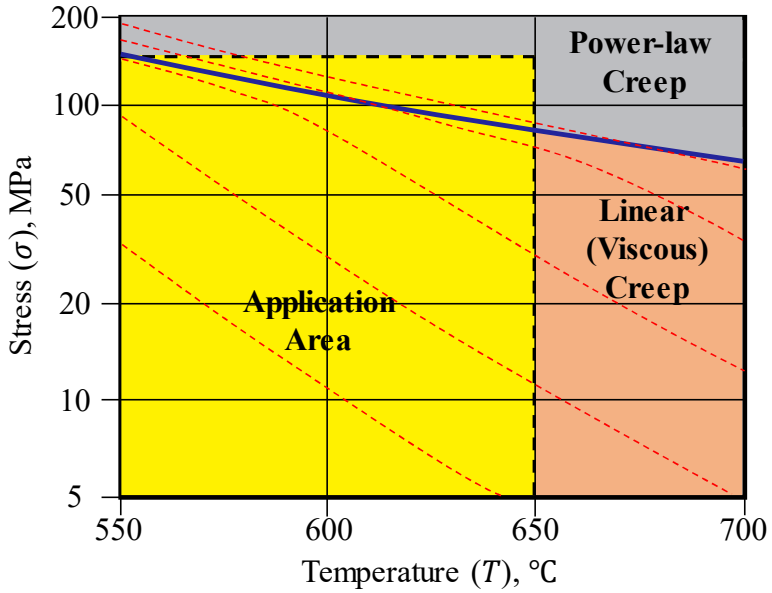

Figure 2.4 – Creep deformation mechanism map 9Cr-1Mo-V-Nb (P91) steel [16].

Using the deformation mechanisms as base theory various models are design and can predict many creep behaviors. There are life-prediction models that predict creep, fatigue, and

creep-fatigue rupture. On the other hand, there is constitutive laws that model creep, cyclic, and unified viscoplasticity. Amongst various efforts, there are several models describing the steady-state creep (secondary creep) by using the minimum-creep-strain rate this behavior would be discussed as well as creep deformation models and continuum damage mechanics models (CDM).

2.3.1 Minimum-creep-strain-rate (MCSR)

Since 1929, the MCSR was one of the earliest creep parameters measured as discussed by Norton who proposed a power-law to describe such behavior [19]. Many stress-dependence models to describe MCSR have been developed and some of the most common are listed in Table 2.1 [20].

Table 2.1 – Minimum-creep-strain-rate (MCSR) models [20, 25].

Source	MCSR Model
Norton, 1929 [19]	$\dot{\varepsilon}_{\min} = A\left(\frac{\sigma}{\sigma_0}\right)^n$
Simplified Norton, 1929 [19]	$\dot{\varepsilon}_{\min} = A\sigma^n$
Nadai, 1931 [21]	$\dot{\varepsilon}_{\min} = A\exp\left(\frac{1}{\sigma_0} + c\sigma\right)$
Soderberg, 1936 [22]	$\dot{\varepsilon}_{\min} = A\left\{\exp\left(\frac{\sigma}{\sigma_0}\right) - 1\right\}$
McVetty, 1943 [23]	$\dot{\varepsilon}_{\min} = A\sinh\left(\frac{\sigma}{\sigma_0}\right)$
Dorn, 1955 [24]	$\dot{\varepsilon}_{\min} = A\exp\left(\frac{\sigma}{\sigma_0}\right)$
Johnson-Henderson-Kahn (JHK), 1936 [25]	$\dot{\varepsilon}_{\min} = A_1\left(\frac{\sigma}{\sigma_0}\right)^{n_1} + A_2\left(\frac{\sigma}{\sigma_0}\right)^{n_2}$
Garofalo, 1965 [26]	$\dot{\varepsilon}_{\min} = A\left\{\sinh\left(\frac{\sigma}{\sigma_0}\right)\right\}^n$

Wilshire, 2007 [60-61].	$\dot{\varepsilon}_{\min} = \left[-\ln\left(\frac{\sigma}{\sigma_{TS}}\right) \Big/ k_2 \right]^{\frac{1}{v}} \exp\left(\frac{-Q_c^*}{RT}\right)$

The base theory of the MCSR models comes from three deformation mechanism which are the diffusional-flow the power-law and breakdown illustrated in Figure 2.5. Diffusional flow, also known as the Harper-Dorn creep, is separated in the Nabarro-Herring and coble creep [20].

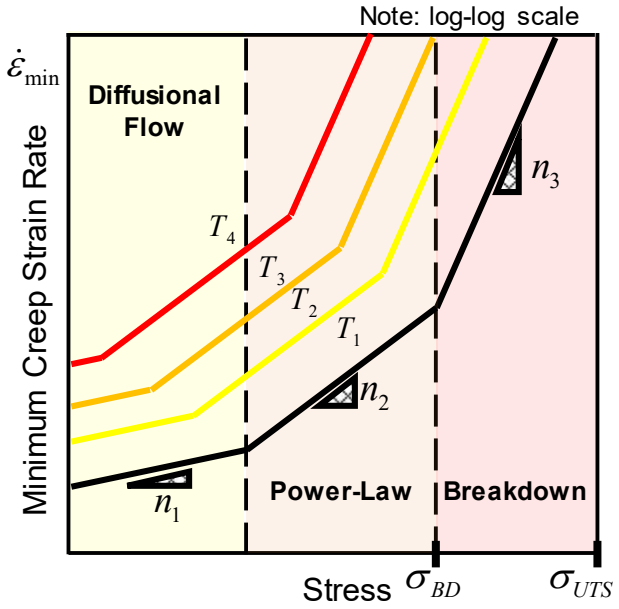

Figure 2.5- Master curve of the minimum-creep-strain-rate based on Norton-power law [20]

The Nabarro-Herring theory or bulk diffusion indicates that there is diffusion through the lattice and grain boundaries. As grain size increases the creep rate typically decreases. The flow of vacancies through the lattice is expressed in the following form

$$\dot{\varepsilon}_{NH} = \frac{A_{NH} D_L G b}{kT} \left(\frac{b}{d} \right)^2 \left(\frac{\sigma}{G} \right) \tag{2.5}$$

where A_{NH} is a dimensionless constant typically 28, D_L is the lattice diffusion coefficient, G is the shear modulus, b is the magnitude of the Burgers vector, k is the Boltzmann's constant, T is the absolute temperature, d is grain size, and σ is flow stress applied to d [17].

Grain boundary diffusion considers flow vacancies along grain boundaries instead. Greater grain size influences the creep rate. Coble proposed an equation to express this behavior in the following form

$$\dot{\varepsilon}_{CO} = \frac{A_{CO} D_{GB} G b}{kT} \left(\frac{b}{d} \right)^3 \left(\frac{\sigma}{G} \right) \tag{2.6}$$

where material constants are the same as Nabarro-Herring; except where, $A_{co} = 33$ and D_{GB} is the grain boundary diffusion coefficient [17].

Dislocation creep is vacancy absorption by dislocation core causing a movement of one atomic space where lattice boundary is diffuse. This causes a specimen or component to climb and glide. Power-law creep is associated with this behavior and is expressed as follows

$$\dot{\varepsilon}_{PL} = \frac{A D_L G b}{kT} \left(\frac{\sigma}{G} \right)^n \tag{2.7}$$

where all material constants remain the same as Nabarro-Herring and Coble and $n \geq 3$ [17,18]. Although these models are presented there is still some controversy as if diffusion flow really exists [27]. Some argue that diffusion flow is only true for pure metals, others sustain is true for all alloys, and some considered as an inexistent mechanism. As a result the exploration on other mechanisms is necessary.

Considering the power-law deformation mechanism the Norton-power law form arrives. The Norton-power law is one of most classic models for MCSR and commonly is shown in the following form

$$\dot{\varepsilon}_{\min} = A\left(\frac{\sigma}{\sigma_0}\right)^n \tag{2.8}$$

where A and n are unitless material constant, σ_0 normalizes stress also known as activation stress and has units of MPa . A most simplified form of the Norton-power law is given without the normalized stress shown as

$$\dot{\varepsilon}_{\min} = A\sigma^n \tag{2.9}$$

where now A must be in units of MPa^{-n} [19]. Both material constants A and n exhibit temperature-dependency. This means that the constants obtained at low stress levels are different from those obtained at high levels as shown in the n constant on Figure 2.5. If the Norton-power law tries to model across multiple isotherms and stress levels, large levels of uncertainty would arrive. The slope for the distinct n from Figure 2.5, is typically 5 but several authors have discovered that it can range between 2 and 12 depending on the creep resistance of materials [27-34].

Soderberg, McVerry and made contributions to addresses temperature dependency and finally Dorn used an Arrhenius function [24]. Dorn suggested that after the material constant A is modified using the Arrhenius approach, the Norton temperature dependent equation takes the following form

$$\dot{\varepsilon}_{\min} = A\left(\frac{\sigma}{\sigma_0}\right)^n \exp\left(\frac{-Q_c}{RT}\right) \tag{2.10}$$

where Q_c is the apparent creep activation energy in $J\ mol^{-1}$, R is the universal gas constant $8.314\ J\ K^{-1}\ mol^{-1}$. It is observed, that material constants Q_c and n have stress dependence still. There is still a need to resolve this issue in order to model across multiple isotherms and stress levels for decades.

Although the secondary creep regime is the most dominant, using the MCSR equations does not predict failure. Many rupture models are also developed, and the combination of both the MCSR and the creep rupture equations can be used to recreate a complete creep deformation curve. Typical, CDM models are based on these two conditions.

2.3.2Creep Rupture

Creep rupture predictions is one of the major concerns in modeling. There exist time-temperature prediction models, relationships with MCSR, and many others which are summarized in Table 2.2.

Table 2.2 – Creep rupture models [35-36,41,44,60-61].

Source	MCSR Model
Larson-Miller, 1952 [35]	$LMP = T\left(\log t_r + K_1\right)$, $t_r = 10^{\frac{LMP - T \cdot K_1}{T}}$
Monkman Grant, 1956 [36]	$\log\left(t_r\right) + m\log\left(\dot{\varepsilon}_{\min}\right) = k_{MG}$, $t_r = \frac{10^{k_{MG}}}{\dot{\varepsilon}_{\min}}$
Kachanov-Rabotnov, 1967-69 [41-42]	$t_r = \left[\left(\phi+1\right) M \bar{\sigma}_r^{\chi}\right]^{-1}$

Evan-Wilshire (Theta Projection), 1984 [43]	$\varepsilon_F = \theta_1\left(1-e^{-\theta_2 t_r}\right)+\theta_3\left(e^{\theta_4 t_r}-1\right)$, solve for t_r
Omega Method, 1996 [44]	$\frac{t_s}{t_r} = \frac{\dot{\varepsilon} t_s \Omega_p}{\dot{\varepsilon} t_s \Omega_p + 1}$
Wilshire, 2007 [60-61].	$t_r = \left[-\ln(\frac{\sigma}{\sigma_{TS}})\Big/ k_1\right]^{\frac{1}{u}} \exp\left(\frac{Q_c^*}{RT}\right)$

One of the earliest prediction models is the Larson Miller parameter (LMP) model which is a time-temperature model [35]. The LMP model is defined as follows

$$LMP = T\left(\log t_r + K_1\right) \tag{2.11}$$

where LMP is a function of stress, T is the temperature, K_1 is a material constant typically ranging between 10 to 50 [37-39]. Monkman Grant recognized that there exists a relationship between the MCSR and rupture time [36]. Creep fractures appears to be inversely related to the MCSR and is given in the following form

$$\dot{\varepsilon}_{\min} \cdot t_r = M \tag{2.12}$$

where M is just the Monkman Grant constant. Further work from Monkman Grant work leads to the current work from Wilshire. Note that such work is discussed later.

Models such as the Kachanov-Rabotnov, Evans-Wilshire theta projection model, and the Omega Method capture creep ductility which helps model the tertiary creep regime. Many of these models are embedded into continuum damage mechanics-based models which not only capture the ductility, but it also takes in consideration the history of damage in materials.

2.3.3 Creep Deformation Models and CDM

The history of damage in a material causes, in most cases, a loss in mechanical properties and strength [40]. This behavior is typically not captured by previous describe creep models. Continuum damage mechanics (CDM) strives to model creep behaviors applying the history of given materials. Considering this process in damage rate equations CDM models provides accumulated damage, residual life and rupture life at given stress and temperature conditions. As a result, creep deformation and damage are best described by CDM based models. Other creep deformation constitutive equations have been developed nonetheless and a summary of these laws and the regimes modeled are shown in Table 2.3 [41-45].

Table 2.3 – Summary of creep constitutive equations [41-45].

Source	Creep Law	Regimes
Kachanov-Rabotnov, 1967-69 [41-42]	$\dot{\varepsilon}_{cr} = A\left(\frac{\sigma}{1-\omega}\right)^{n},\ \dot{\omega} = \frac{M\sigma^{\chi}}{(1-\omega)^{\phi}}$	Secondary Tertiary
Evans-Wilshire (Theta Projection), 1984 [43]	$\varepsilon = \theta_1\left(1-e^{-\theta_2 t}\right)+\theta_3\left(e^{\theta_4 t}-1\right)$	Primary Secondary Tertiary
Prager, M. (MPC Omega), 1995 [44]	$\dot{\varepsilon}_{cr} = \dot{\varepsilon}_0 \exp\left(\Omega_p \varepsilon\right)$	Secondary Tertiary
Liu and Murakami, 1998 [45].	$\dot{\varepsilon}_{cr} = \frac{3}{2} A\sigma_{eq}{}^{n} \frac{S_{ij}}{\sigma_{eq}} \exp\left(\frac{2(n+1)}{\pi\sqrt{1+3/n}} \cdot \frac{\sigma_1}{\sigma_{eq}} \cdot \omega^{3/2}\right)$ $\dot{\omega} = B\frac{\left(1-\exp\left(-q_2\right)\right)}{q_2}\sigma_r{}^{\chi}\exp\left(q_2\omega\right)$	Secondary Tertiary
Sinh Model 2013, [14]	$\dot{\varepsilon}_{cr} = A\sinh\left(\sigma/\sigma_s\right)\exp\left(\lambda\omega^{3/2}\right)$ $\dot{\omega} = \frac{M\left[1-\exp(-\phi)\right]}{\phi}\sinh\left(\frac{\sigma}{\sigma_t}\right)^{\chi}\exp(\phi\omega)$	Secondary Tertiary

The Kachanov-Rabotnov model came as a contribution between the work of Kachanov introducing phenomenological CDM for damage modeling and Rabotnov incorporated damage into the creep strain rate equation [41-42]. The Kachanov-Rabotnov model for creep strain and damage rate are as follow

$$\dot{\varepsilon}_{cr} = \frac{d\varepsilon_{cr}}{dt} = A\left(\frac{\sigma}{1-\omega}\right)^{n} \tag{2.13}$$

$$\dot{\omega} = \frac{d\omega}{dt} = \frac{M\sigma^{\chi}}{(1-\omega)^{\phi}} \tag{2.14}$$

where A and n are the Norton-power law constants, σ is equivalent stress, M , χ , ϕ are material constants that model the tertiary creep regime. The Kachanov-Rabotnov model has predicted accurately creep deformation, however, is limited on its fundamental forms [40-47]. Kachanov-Rabotnov is considered a local CDM approach which means rupture is achieve when damage variable is unity, however, rupture occurs below unity. The Kachanov-Rabotnov model has stress sensitivity which means that damage rate becomes unrealistically huge near rupture time [40].

The theta-projection model proposed by Evans and Wilshire is a multistage model that connects the primary and tertiary regimes using the material constants [43]. The classic theta-projection model is shown as follows

$$\varepsilon = \theta_1\left(1-e^{-\theta_2 t}\right) + \theta_3\left(e^{\theta_4 t}-1\right) \tag{2.15}$$

where the theta-constants θ_1 and θ_2 generate the primary creep regime and θ_3, θ_4 control the tertiary regime. The theta constants are functions of stress and temperature that are numerical in

nature. A limitation the theta-projection model shows is that a single set of theta values are not always accurate when predicting multiple isotherms and stress levels. There is especially a problem with θ_4 as for long rupture life predictions creep strain becomes very large and if θ_4 is set low underpredictions arrive at an early stage of the creep deformation curve [48].

The MPC Omega model was first introduced by Prager in 1995 [44]. The damage model of the MPC Omega is given as

$$\omega = \frac{t}{t_r} = \frac{\dot{\varepsilon}\Omega_p t}{1 + \dot{\varepsilon}\Omega_p t} \tag{2.16}$$

where t is the current time, t_r is the rupture time, and Ω_p is a material constant susceptible to creep [48]. Material constant Ω_p is obtained through experimental data and by taking the natural logarithm, rearranging, and simplifying [Eq. (2.16)] the following creep strain form is obtained

$$\dot{\varepsilon}_{cr} = \dot{\varepsilon}_0 \exp\left(\Omega_p \varepsilon\right) \tag{2.17}$$

where ε is the current creep strain and the logarithm of both sides is as follows

$$\ln\left(\dot{\varepsilon}_{cr}\right) = \ln\left(\dot{\varepsilon}_0\right) + \varepsilon\Omega_p \tag{2.18}$$

where Ω_p is determined from the slope of $\ln\left(\dot{\varepsilon}_{cr}\right)$ versus ε. If the plot between $\ln\left(\dot{\varepsilon}_{cr}\right)$ and ε determines if the plot does not have a straight line in which at this moment it is not recommended to use the MPC Omega model [48].

As a modification of the Kachanov-Rabotnov model Liu and Murakami creep damage model is obtained [45]. Liu and Murakami model creep and damage models are in the following form

$$\dot{\varepsilon}_{eq} = \frac{3}{2} A {\sigma_{eq}}^{n} \frac{S_{ij}}{\sigma_{eq}} \exp\left(\frac{2(n+1)}{\pi\sqrt{1+3/n}} \cdot \frac{\sigma_1}{\sigma_{eq}} \cdot \omega^{3/2} \right) \tag{2.19}$$

$$\dot{\omega} = B \frac{\left(1-\exp\left(-q_2\right)\right)}{q_2} {\sigma_r}^{\chi} \exp\left(q_2 \omega\right) \tag{2.20}$$

where A, n, B, q_2, and χ are material constants, σ_r is the rupture stress, $\dot{\varepsilon}_{eq}$ and σ_{eq} are the equivalent strain and stress respectively, S_{ij} is the deviatoric stress and ω is damage. In this case, when ω reaches a critical value, typically 0.99, failure is assumed to occurred [46]. Note that through this work the Sinh model is developed which is discussed later.

Many more models have been developed for both MCSR and creep deformation which are not listed. There is a need to determine which model is best and produce accurate predictions. Two additional models are discussed on future chapters which are used to develop the new constitutive model.

CHAPTER 3: MATERIAL P91

3.1 Material Properties, Chemical Composition, Material Database

The subject material is 9Cr-1Mo-V-Nb steel better known as P91 alloy. Some applications for P91 are pipelining, boiling components, and steam generators due to the high resistance to stress corrosion and oxidation [49-50]. Alloy P91 is a ferritic-martensitic steel due to the 9 wt% Cr and with the addition of Nb and V creep strength increases [51]. The microstructure of a P91 tube is obtained from the National Institute of Materials Science (NIMS) database and is illustrated in Figure 3.1, where the material has been heat treated to MGC. It is observed that there are precipitate carbides, which most typically are $M_{23}C_6$, located at the grain boundaries [52-53]. There are carbonitrides finely distributed within the ferritic-martensitic matrix as well. The microalloying elements Nb, V, and Mo are the ones that formed these fine and stable carbides and carbonitrides. These prevents dislocation within the grain boundaries and retains finer grains during austenization delaying plastic deformation due to grain boundary sliding.

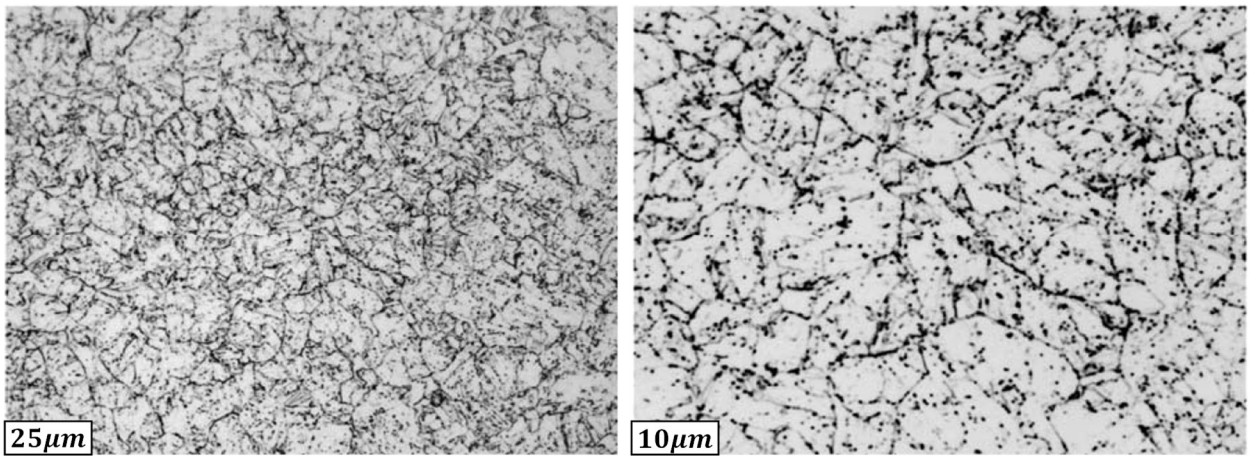

Figure 3.1 – Microstructure of 9Cr-1Mo-V-Nb (P91) steels tube MGC at center of wall thickness [53].

The NIMS nominal chemical composition in mass percent of alloy P91 is reported in Table 3.1 [53]. Notice that the chemical composition varies between the material forms of tube, plate, and pipe. Distinct chemical compositions mean that the material properties are different and must be considered in modeling calibration processes. Even when the same material form is considered, the heat treatment defines many of the material properties.

Table 3.1 - Nominal chemical composition (mass percent) of tube, plate and pipe for 9Cr-1Mo-V-Nb (P91) [53].

Element	Tube	Plate	Pipe
Fe	Bal.	Bal.	Bal.
C	0.07-0.14	0.06-0.15	0.08-0.12
Si	0.20-0.50	0.18-0.56	0.20-0.50
Mn	0.30-0.60	0.25-0.66	0.30-0.60
P	≤0.020	≤0.025	≤0.020
S	≤0.010	≤0.012	≤0.010
Ni	≤0.40	≤0.43	≤0.40
Cr	8.00-9.50	7.90-9.60	8.00-9.50
Mo	0.85-1.05	0.80-1.10	0.85-1.05
V	0.18-0.25	0.16-0.27	0.18-0.25
Nb*	0.06-0.10	0.05-0.11	0.06-0.10
N	0.30-0.070	0.025-0.080	0.030-0.070
Al*	≤0.04	≤0.05	≤0.04
	≤0.02	≤0.02	≤0.02
Ti*	-	-	-
	≤0.01	≤0.01	≤0.01
Zr*	-	-	-
	≤0.01	≤0.01	≤0.01

The heat treatments for each material form for alloy P91 is presented in Table 3.2 which is taken from the NIMS database [53]. Heat treatments are denoted as; MGA, MGB, MGC, MGD, MGF, and MGD for tube, MgA, MgB, MgC, MgD for plate, and MGQ for pipe. Each batch of material is reported alongside with its type of melting, process, thermal history, and the Rockwell hardness (HRC). The types of melting are basic electric arc (BEA) furnace, LD converter (LDC),

and top and bottom blown converter (TBBC). The processing is either hot extruded and cold drawn, how extruded, and hot rolled with air cooling (AC) or furnace cooling (FC).

Table 3.2- Details of heat treatment for alloy 9Cr-1Mo-V-Nb (P91) in tube, plate, and pipe form [53].

Tube			
Heat Treatment	Type of Melting	Processing and thermal history	Rockwell hardness (HRC)
MGA	BEA	Hot extruded and cold drawn 1045 $^{\circ}C$ /10 min AC 780 $^{\circ}C$ /60 min AC	16
MGB	BEA	Hot extruded and cold drawn 1050 $^{\circ}C$ /60 min AC 760 $^{\circ}C$ /60 min AC	16
MGC	BEA	Hot extruded and cold drawn 1050 $^{\circ}C$ /10 min AC 765 $^{\circ}C$ /30 min AC	18
MGD	LDC	Hot extruded and cold drawn 1050 $^{\circ}C$ /10 min AC 780 $^{\circ}C$ /40 min AC	18
MGF	BEA	Hot extruded 1045 $^{\circ}C$ /60 min AC 780 $^{\circ}C$ /60 min AC	18
MGG	TBBC	Hot rolled 1050 $^{\circ}C$ /15 min AC 790 $^{\circ}C$ /60 min AC	18
Plate			
Heat Treatment	Type of Melting	Processing and thermal history	Rockwell hardness (HRC)
MgA	BEA	Hot rolled 1050 $^{\circ}C$ /10 min AC 770 $^{\circ}C$ /60 min AC 740 $^{\circ}C$ /8.4 h FC	13

MgB	BEA	Hot rolled 1050 °C /10 min AC 770 °C /60 min AC 740 °C /60 min FC	14
MgC	LDC	Hot rolled 1060 °C /90 min AC 760 °C /60 min AC 730 °C /8.4 h FC	17
MgD	LDC	Hot rolled 1050 °C /30 min AC 780 °C /30 min AC	16

Pipe

Heat Treatment	Type of Melting	Processing and thermal history	Rockwell hardness (HRC)
MGQ	BEA	Hot rolled 1060 °C /60 min AC 780 °C /60 min AC	15

Considering each material form and knowing that each heat treatment produces different properties the tensile strengths, σ_{TS} given in Table 3.3. The average tensile strength for each form is given across the different heat treatments. The remaining values that are not given in the NIMS database but that are considered on this study are interpolated.

Table 3.3 - Average tensile strength for alloy P91 for tube, plate and pipe interpolating and using the NIMS database [53]

	Average Tensile Strength, σ_{TS}		
Temperature (°C)	Tube (MPa)	Plate (MPa)	Pipe (MPa)
100	658.33	635.75	621
200	620.83	589.25	583
300	592.50	561.00	554
400	568.67	492.25	533
450	527.67	516.75	512
500	486.67	469.75	464
550	418.00	414.00	402

575	382.09*	375.5*	367.5*
600	346.17	337.00	333
625	309.09*	306.13*	299.5*
650	272.00	275.25	266
675	237.25*	240.25*	483
700	202.50	205.25	200

*tensile strengths that are interpolated

In total, 200 stress-rupture and 350 MCSR experimental data points are available which are gathered and illustrated in Figure 3.2. These available points are used to calibrate the Wilshire equations that are later describe in Chapter 4. Both stress-rupture and MCSR data are presented with respect to the isotherm. The heat treatment and the material forms are not considered in Figure 3.2. Note this is important as Chapter 4 considers the material form and the plot is separated into tube, plate, and pipe and Chapter 5 considers the specific heat treatment. Each material form has some sort of available data for calibration and for further post-audit validation. The available data and for both stress-rupture and MCSR for tube, plate, and pipe as well as the available isotherms is presented in Table 3.4. Notice that for each material form there is a different number of isotherms for stress-rupture and MCSR; tube has five isotherms for stress-rupture and eight for MCSR, plate has five and eight isotherms for stress-rupture and MCSR respectively, and pipe has five and seven for stress-rupture and MCSR.

Table 3.4 – Available datapoints for stress-rupture and MCSR obtained from NIMS and Figure 3.2 [53]

	Tube	Plate	Pipe
Stress-Rupture Available Data	80	80	40
Stress-Rupture Isotherms (°C)	500, 550, 600, 650, and 700	450, 500, 550, 600, and 650	450, 500, 550, 600, and 650

MCSR Available Data	180	130	30
MCSR Isotherms (°C)	500, 550, 575, 600, 625, 650, 675 and 700	450, 500, 550, 575, 600, 625, 650, and 700	500, 550, 575, 600, 625, 650, and 700

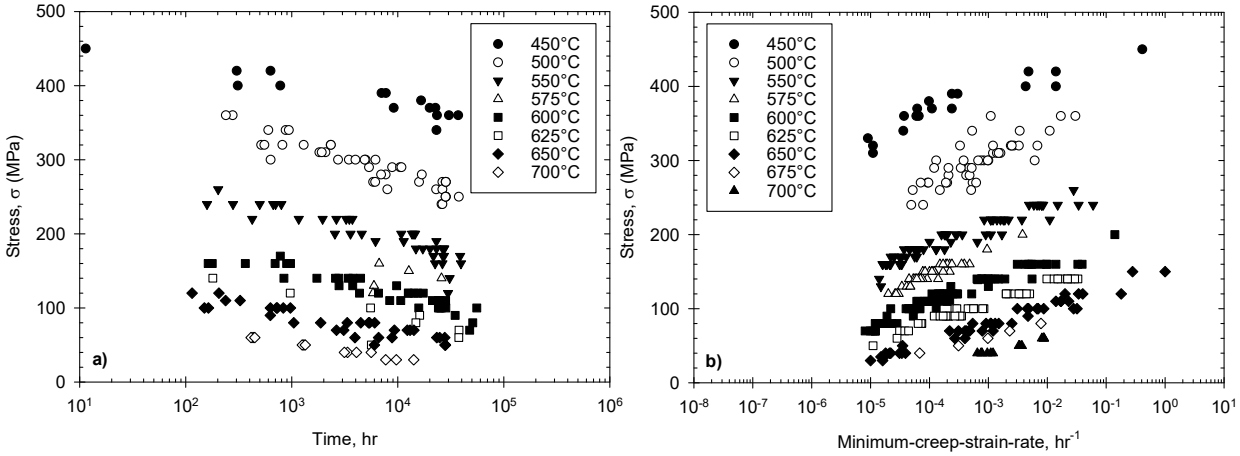

Figure 3.2 – Data gather from the NIMS database for a) stress-rupture and b) minimum-creep-strain-rate for multiple forms, isotherms, and heat treatments [53].

Creep deformation data is also collected from the work of Kimura et al for P91 as illustrated in Figure 3.3 [54]. The data is given for a single isotherm 600°C and six different stresses (100, 110, 120, 140, 160, and 200 MPa). The data expands for more than 10^4 hours which is more than three years of data. The data for P91 in this study is reported to be heat treated as MGC. The chemical composition is specified in this study and is shown in Table 3.5. The material is assumed to be in tube form due to the description of the chemical composition and which together with the heat treatment matches those presented in the NIMS database. In this particular case for alloy P91, yield stress of the material at 600°C is $289\ MPa$ and the $\sigma_{TS} = 357\ MPa$.

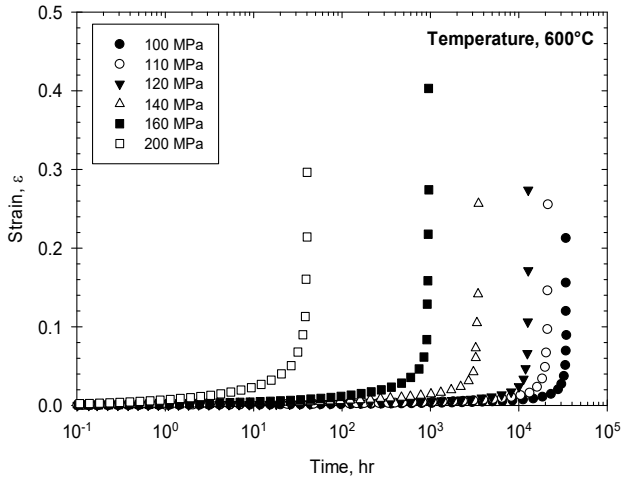

Figure 3.3 - Creep deformation curves for alloy P91 at 100, 110, 120, 140, 160, and 200 MPa and 600°C [54]. Note the x-axis is on a logarithmic scale.

Table 3.5 – Nominal chemical composition (mass percentage) of Heat MGC for alloy 9Cr -1Mo-V-Nb (P91) [54]

Element	Mass percent (mass%)
Fe	Bal.
C	0.09
Si	0.29
Mn	0.35
P	0.009
S	0.002
Ni	0.28
Cr	8.70
Mo	0.90
Cu	0.032
V	0.22
Nb*	0.072
N	0.044
Al*	0.001

CHAPTER 4: APPLICATION WILSHIRE STRESS-RUPTURE AND MCSR IN TUBE, PLATE, AND PIPE FORM

4.1 Introduction and Methodology

Through the background and literature it is understood that numerous models have been developed to predict different creep behaviors. Amongst existing models, the Wilshire model has emerged as a promising choice for extrapolation. The Wilshire model was introduced to predict the stress-rupture and MCSR behavior of materials and the model is well-accepted due to the explicit description of stress- and temperature-dependence allowing predictions across isotherms and stress levels.

There is a need to determine to what extent does the material form affect the predictions of the Wilshire model and the calibrated material constants. Considering the work done by Holdsworth, the material characteristics each form creates a different set of material constants affecting the accuracy of the Wilshire models. Also, data distribution is considered to assess the model's behavior for each material form but rather than considering the complete dataset for model fitting, this study considers the short-term data for the calibration and the predictive abilities are vetted with the long-term data [55].

The objective of this chapter is to assess the stress-rupture and MCSR prediction models for Wilshire at multiple isotherms, stress levels, and material forms. The stress-rupture and MCSR predictions are generated for alloy P91 in tube, plate, and pipe form. Data used from the National Institute of Materials Science (NIMS) material database for alloy P91 at multiple isotherms as describe in Chapter 3 and illustrate in Figure 3.2. Following the establish method from Wilshire the model is calibrated using shot-term data ($<10^4$ hours) and post-audit validation is performed

using long-term data ($\geq 10^4$ hours) to vet the extrapolations accuracy of each form at different isotherms. This chapter discusses, as well, the origins of the Wilshire model and how the model is calibrated.

4.2 Origins of the Wilshire Model

To understand the Wilshire model, it is necessary to examine two classic models previously discussed: the Norton-power law for MCSR and the Monkman-Grant law for rupture prediction mention previously [19,56-59]. The Norton-power law models the MCSR, $\dot{\varepsilon}_{\min}$ as follows

$$\dot{\varepsilon}_{\min} = A\sigma^n \exp\left(-\frac{Q_c}{RT}\right) \tag{4.1}$$

where it takes a similar form as [Eq. (2.10)] but using the simplified Norton. The material parameters A, n, and Q_c are functions of stress and temperature; suggesting that different creep mechanism become dominant at different stress and temperature regimes. To mitigate this problem, stress can be normalized by the ultimate tensile strength, σ_{TS} as follows

$$\dot{\varepsilon}_{\min} = A^*\left(\frac{\sigma}{\sigma_{TS}}\right)^n \exp\left(-\frac{Q_c^*}{RT}\right) \tag{4.2}$$

where the coefficient, A^* and creep activation energy, Q_c^* are stress- and temperature-independent [60-61]. Unfortunately, stress-dependence persists in the n constant due to the nonlinearity observed in normalized stress-rupture data when plotted on a log-log scale. The change in the n constant is associated with distinct creep deformation mechanism such as diffusional flow (Harper-Dorn), power-law, and breakdown as illustrated in Figure 2.5 [60-62].

The Monkman-Grant law arises from the inverse relationship between the minimum-creep-strain-rate, $\dot{\varepsilon}_{\min}$ and rupture time, t_f as shown in [Eq. (2.12)]. Subsequently, rupture time can be predicted by combining the Norton-power and Monkman-Grant laws, [Eq. (4.2)] into [Eq. (2.12)] and rearranging as follows

$$t_f = M\left[A^*(\frac{\sigma}{\sigma_{TS}})^n \exp(-\frac{Q_c^*}{RT}) \right]^{-1} \tag{4.3}$$

where $\dot{\varepsilon}_{\min}$ and t_f predictions take the same functional form distinguished by different coefficients and exponents.

4.3 The Wilshire Model

Wilshire determine that Norton-power and Monkman-Grant laws have limitations predicting creep behaviors [63-66]. The stress-dependence of the stress exponent, n persists where n can varied from $n>5$ at high-stress to $n\cong 1$ at low-stress [60-61, 67]. Diffusional flow is theorized to exist at low-stress $\left(\sigma<0.5\sigma_{YS}\right)$; however, literature suggests that diffusion flow does not exist [62]. Rather, diffusion flow is an artefact of the methodology being utilized (i.e. Norton-power law) [67]. Note, this problem persists in the Wilshire model where the material constants may need to be segregated into low-, intermediate-, and high-stress regimes depending on the creep data [61,63]. Based on these observations, Wilshire proposed alternative rupture time, t_f and minimum-creep-strain-rate, $\dot{\varepsilon}_{\min}$ laws as follows

$$\frac{\sigma}{\sigma_{TS}} = \exp\left(-k_1\left[t_f \exp\left(-\frac{Q_c^*}{RT} \right) \right]^u \right) \tag{4.4}$$

$$\frac{\sigma}{\sigma_{TS}} = \exp\left(-k_2 \left[\dot{\varepsilon}_{\min} \exp\left(\frac{Q_c^*}{RT} \right) \right]^v \right) \tag{4.5}$$

where k_1 (in hr^{-u}), u, k_2 (in $\left(hr^{-1}\right)^{-v}$), and v are material constants. The $\dot{\varepsilon}_{\min}$ and t_f predictions take the same functional form and are distinguished by different coefficients (k_1, k_2) and exponents (u, v) [60-61,63-66,68]. Note the $\dot{\varepsilon}_{\min}$ prediction lacks a negative sign ahead of Q_c^*. An analytical solution to determine the material constants of the Wilshire model is well established.

4.4 Calibration Methods of the Wilshire Model

The six material constants of the Wilshire model (σ_{TS}, Q_c^*, k_1, u, k_2, and v) can be analytically determined using the approach illustrated in Figure 4.1 through Figure 4.3. Three isotherms of creep data or more are required for calibration. First, monotonic tensile tests shall be performed at each isotherm to gather the ultimate tensile strength, σ_{TS}. Next, creep tests at fixed stress ratio, σ_i / σ_{TS} $i = 1, 2, 3$ shall be performed per isotherm. Creep activation energy, Q_c^* appears in both [Eq. (4.4)] and [Eq. (4.5)] and must be determined first. To obtain Q_c^*, take a fixed stress ratio and plot $\ln(\dot{\varepsilon}_{\min})$ or $\ln(t_f)$ versus $1/T$ as illustrated in Figure 4.2. The fixed stress ratio enables [Eq. (4.4)] and [Eq. (4.5)] to be simplified such that the slope in Figure 4.2 reveals the creep activation energy, [67,69-70]. The remaining constants arise from plotting $\ln[-\ln(\sigma/\sigma_{TS})]$ versus $\ln[t_f \exp(-Q_c^*/RT)]$ and $\ln[-\ln(\sigma/\sigma_{TS})]$ versus $\ln[\dot{\varepsilon}_{\min} \exp(Q_c^*/RT)]$ as illustrated in Figure 4.3 (a) and (b). The stress-rupture constants k_1 and u and the MCSR constants k_2 and v

are the y-intercept and slope in Figure 4.3 (a) and (b) respectively [63-66]. When properly calibrated, the Wilshire model is one of the best models for predicting the stress-rupture and MCSR over a wide range of temperatures and stress when compared to existing models [67,69].

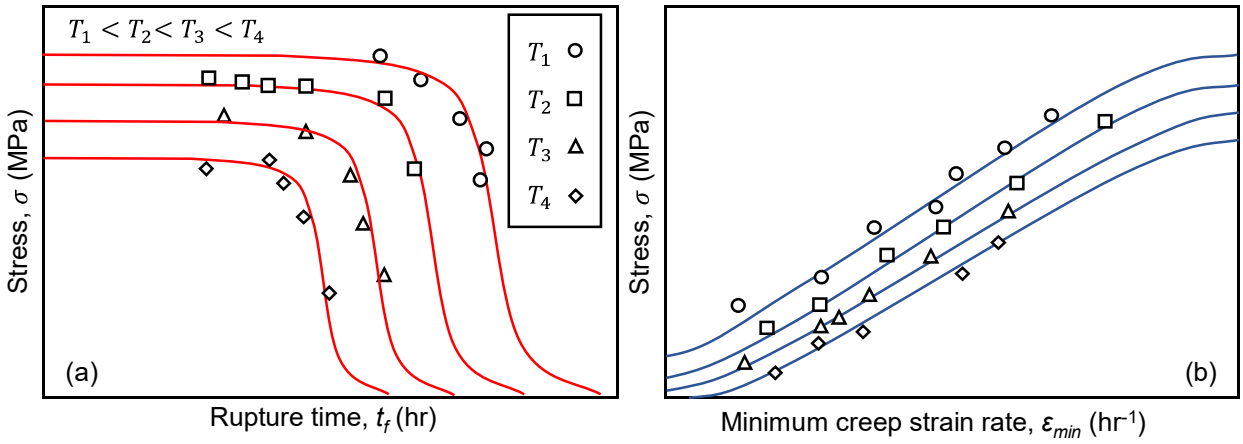

Figure 4.1- Illustration of (a) stress-rupture and (b) minimum-creep-strain-rate using Wilshire model.

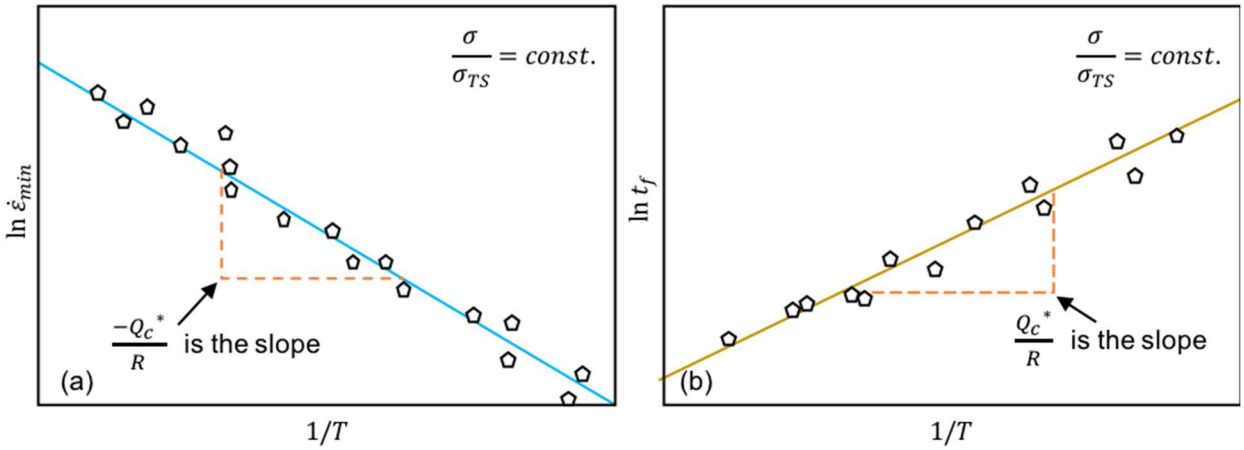

Figure 4.2 - Analytical calibration of the creep activation energy, Q_c^* using either (a) stress rupture data or (b) minimum-creep-strain-rate data respectively.

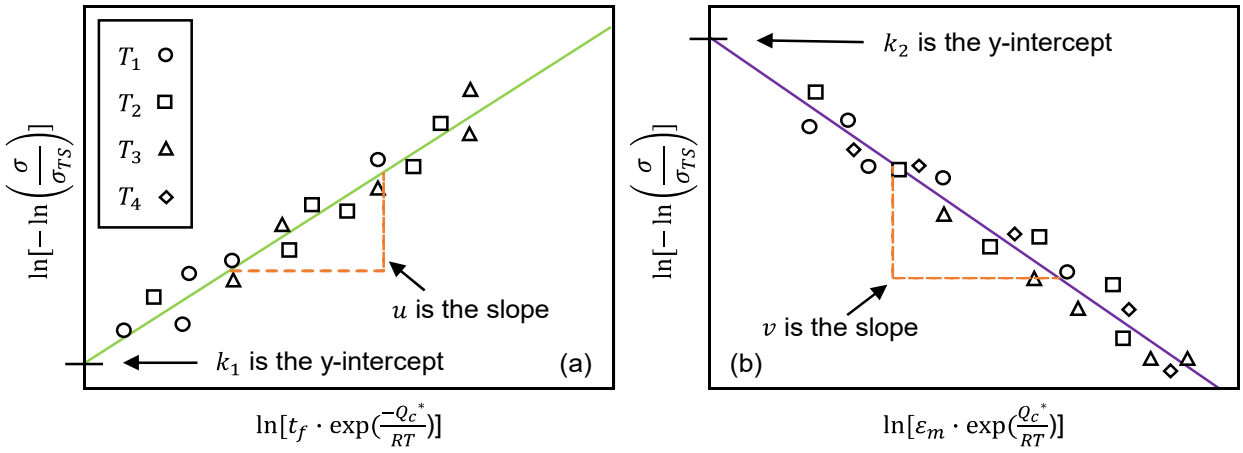

Figure 4.3 - Analytical calibration of (a) stress-rupture constants k_1 and u using [Eq. (4.4)] and (b) minimum-creep strain-rate constants k_2 and v using [Eq. (4.5)].

4.5 Material Constants

The material constants of the Wilshire model $(\sigma_{TS}, Q_c^*, k_1, u, k_2,$ and $v)$ are obtained for each form using the described calibration method. The average tensile strengths, σ_{TS} listed in Table 3.3 are employed everywhere except when calculating Q_c^* where the heat-specific strengths are employed.

The Q_c^* is determined by plotting $\ln(t_f)$ versus $1/T$ at a constant stress ratio σ/σ_{TS} as illustrated in Figure 4.2 (b). The Q_c^* plots for tube, plate, and pipe alloy P91 are provided in Figure 4.4 outline as (a), (b), and, (c) respectively. The Q_c^* is calculated for several stress ratios and are shown in Table 4.1 including the mean values, the standard deviation, and the coefficient of variation (COV).

It is observed that the variation between material form and even from stress ratio is significant. This is important because as shown in Figure 4.3 the Wilshire material constants

$(k_1, u, k_2, \text{ and } v)$ are determined using the creep activation energy. The curvature of the model and the extrapolations are determine using this material constants so a small change of Q_c^* constitutes uncertainty. Using the rounded mean value, the remaining material constants are determined. Note that if a single material batch of a specific heat treatment is needed then the predictive capabilities might not be as good. It is recommended that if the heat treatment and material properties of a material are given then a recalibration is needed for better predictions.

Table 4.1 – Creep activation energy, Q_c^* at each stress ratio with the standard deviation, the mean value, and the coefficient of variation (COV)

	Tube	Plate	Pipe
0.3 ($kJmol^{-1}$)	322.62	-	-
0.4 ($kJmol^{-1}$)	213.35	363.38	276.96
0.5 ($kJmol^{-1}$)	177.25	266.75	200.03
0.6 ($kJmol^{-1}$)	198.86	229.83	196.56
Mean	228.02	286.65	224.52
St. Deviation	64.7875	68.9638	45.4504
COV	0.2841	0.2406	0.2024

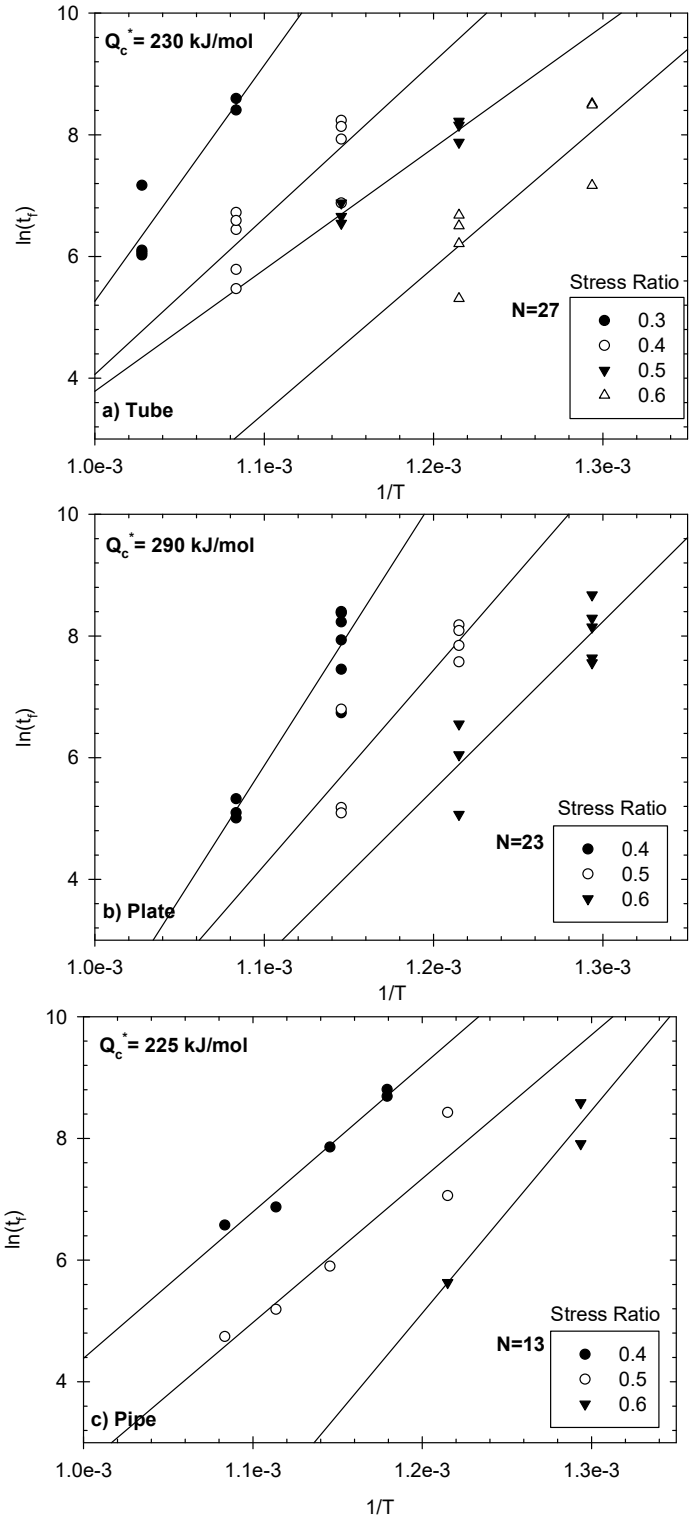

Figure 4.4 - Creep activation energy, Q_c^* calibration for (a) **tube** $Q_c^* \cong 230\ kJmol^{-1}$ (b) **plate** $Q_c^* \cong 290\ kJmol^{-1}$ and (c) **pipe** $Q_c^* \cong 225\ kJmol^{-1}$.

The $(k_1, u, k_2, \text{and } v)$ material constants are found analytically as illustrated in Figure 4.3. The stress-rupture and MCSR calibration plots for tube, plate, and pipe alloy P91 are provided from Figure 4.5 to Figure 4.7. The material constants for tube, plate, and pipe are summarized in Table 4.2.

Table 4.2 – Summary of the material constants Q_c^*, k_1, u, k_2, and v for the tube, plate and

Constant	Tube	Plate	Pipe
$Q_{c\ avg}^{*}$ $(kJmol^{-1})$	230	290	225
$k_1 (hr^{-u})$	50.87	98.36	56.46
u (unitless)	0.1688	0.1441	0.1761
$k_2 \left(hr^{-1}\right)^{-v}$	50.71	88.31	54.22
v (unitless)	-0.1584	-0.1357	-0.1661

The constants for the three forms are different even though the material remains the same. Besides the variation on the creep activation energy, defects of microstructures that presents at different heat treatments and manufacturing processes from form to form affect the material constants. The chemical composition of the material is an indicator of this change. The three forms have different chemical compositions as shown in Table 3.1 and depending of the heat process the chemical composition changes. The plate is the form that has the most significant change for the chemical composition. The plate is also the one that has the highest Q_c^* which can relate to less defect as is the easiest to manufacture.

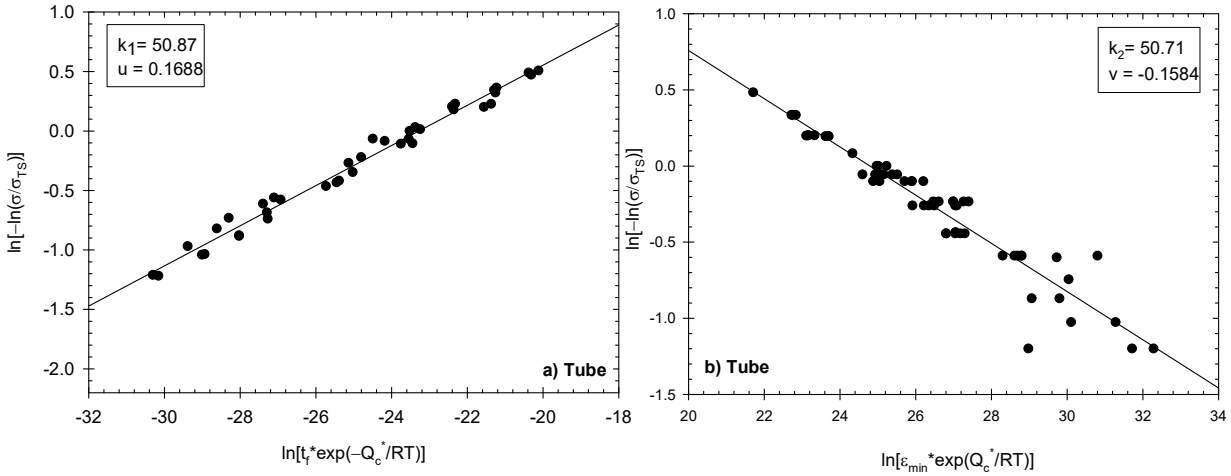

Figure 4.5 – Calibration of tube material constants for a) stress-rupture where $k_1 = 50.87$ and $u = 0.1688$ using [Eq. (4.4)] and b) MCSR $k_2 = 50.71$ and $v = -0.1584$ where using [Eq.(4.5)].

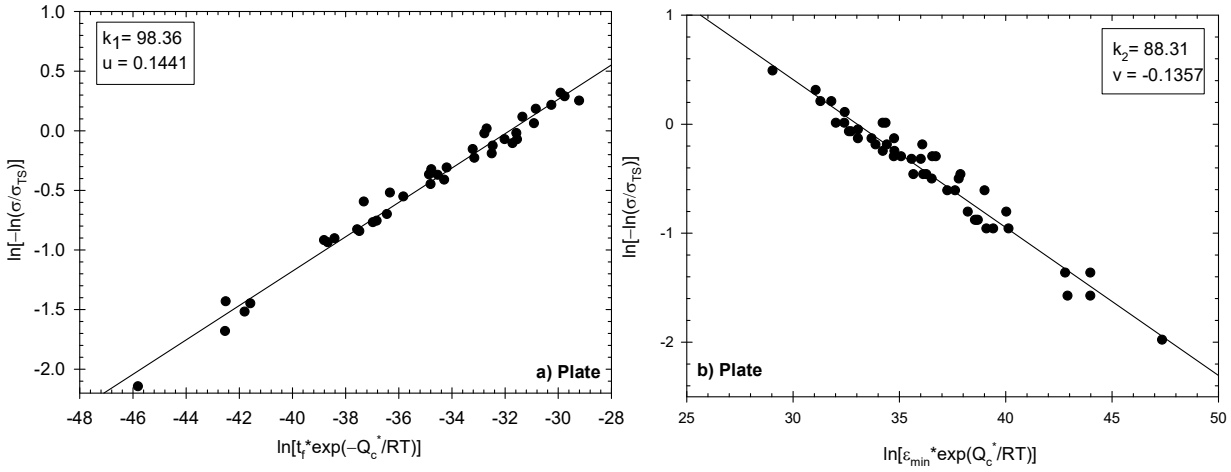

Figure 4.6 – Calibration of plate material constants for a) stress-rupture where $k_1 = 98.36$ and $u = 0.1441$ using [Eq. (4.4)] and b) MCSR $k_2 = 88.31$ and $v = -0.1357$ where using [Eq.(4.5)].

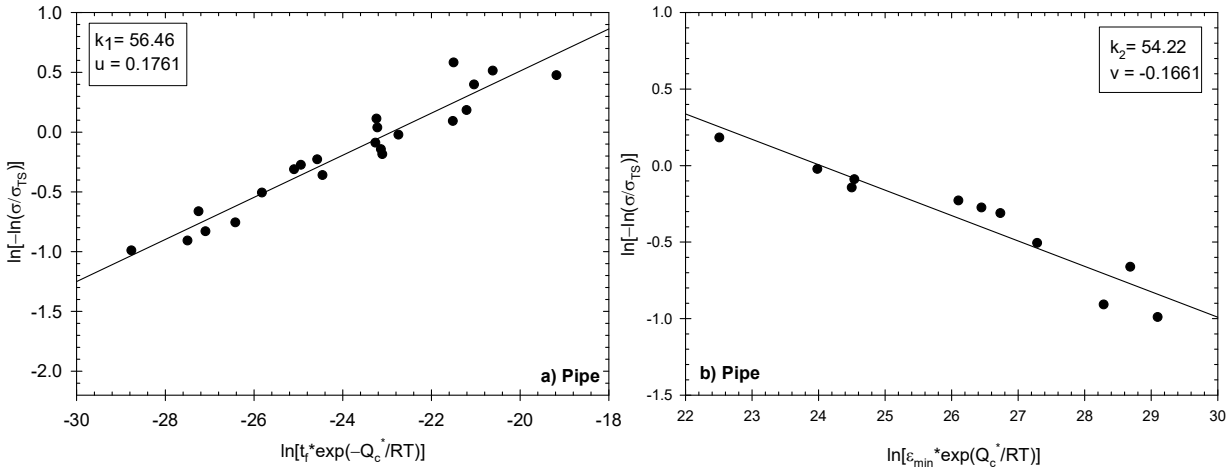

Figure 4.7 - Calibration of pipe material constants for a) stress-rupture where $k_1 = 56.46$ and $u = 0.1761$ using [Eq. (4.4)] and b) MCSR $k_2 = 54.22$ and $v = -0.1661$ where using [Eq.(4.5)].

4.6 Stress-Rupture Prediction Model and Design Maps

The material constants (Q_c^*, k_1, and u) obtain from Table 4.2 are plug into the stress-rupture Wilshire [Eq. (4.4)] to obtain the predictive model. The resulting predictions are shown in Figure 4.8 a), Figure 4.9 a), and Figure 4.10 a) for tube, plate, and pipe respectively. The vertical dashed line across the graph represents the division between the data used in the calibration process and the extrapolations that were made. The numbers used for calibration did not exceed 5000, 5500, and 6000 hours for the tube, plate, and pipe respectively. These limits are set as it does not exceed (10^4) from the available data which is the typical separation point from short-term to long-term.

Using the stress-rupture model [Eq. (4.4)] as well, design maps are created for design engineers. Design maps are contour plots that contains variables of interest for design engineers. In this particular case, the design map has stress as the y-axis in MPa, the x-axis is the temperature

in $^{\circ}C$, and the contour value z is the predicted rupture time, t_r . The material constants Q_c^*, k_1, and u as well as the, σ_{TS} are implemented into the stress-rupture equation at different combinations of stress and temperature. The label lines are the contour lines predicting rupture time and the bold line with white spacing is the UTS of the material.

Simulations are performed from 0 to 550 MPa and from 400 to 700 $^{\circ}C$ for the tube, plate and pipe as illustrated in Figure 4.8 b), Figure 4.9 b), and Figure 4.10 b) respectively. It is observed that the plate has the most "infinite life" of the three with a larger area for predictions greater than 10^7. The design maps are tools for engineers but also define which form performs best at different conditions. The maps have areas that are similar, or have small variance, which is also an indicator that at some conditions a design engineer can choose the three form and would have a similar rupture life.

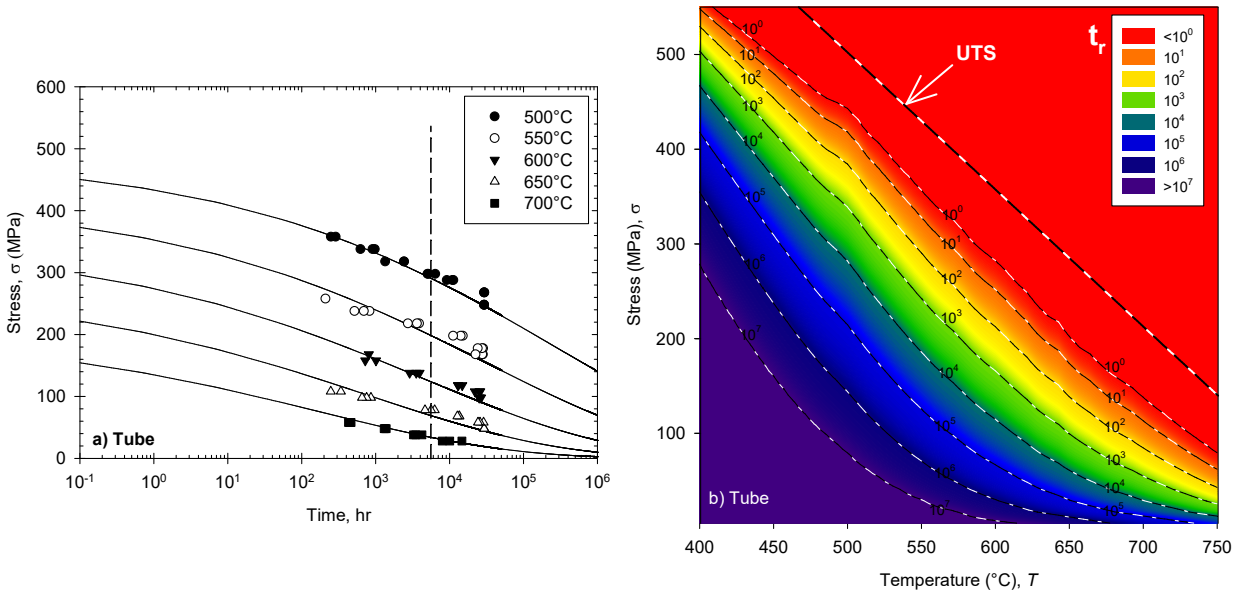

Figure 4.8 – Using Wilshire [Eq. (4.4)] in a tube a) stress-rupture predictions for alloy P91 and b) design rupture maps are obtained.

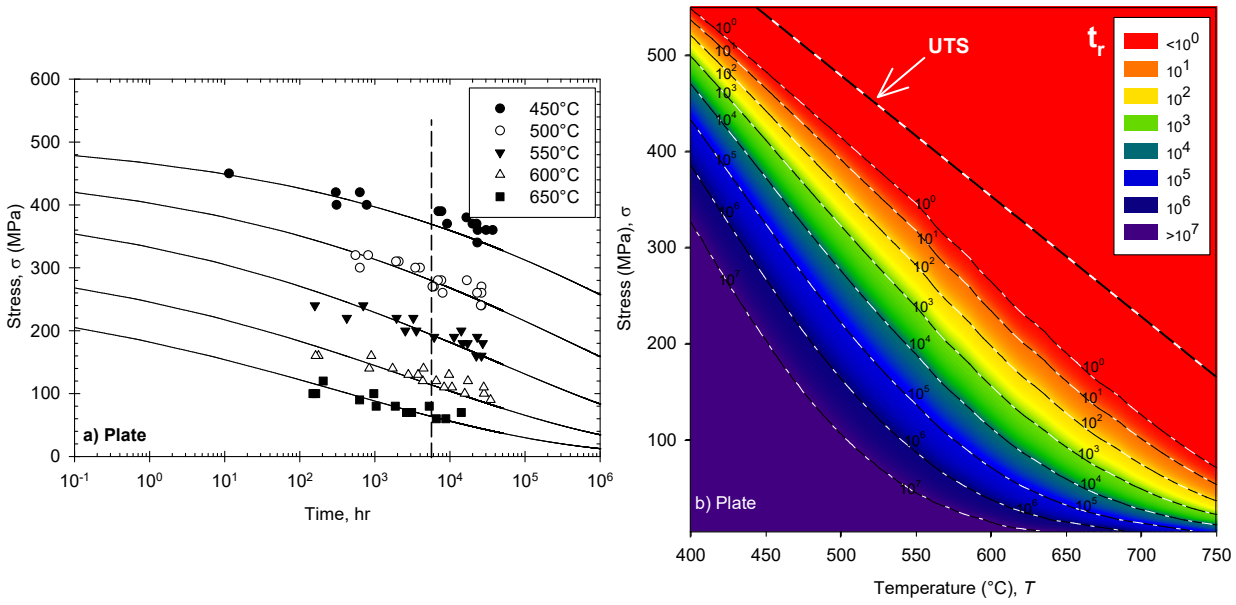

Figure 4.9 – Using Wilshire [Eq. (4.4)] in a plate a) stress-rupture predictions for alloy P91 and b) design rupture maps are obtained.

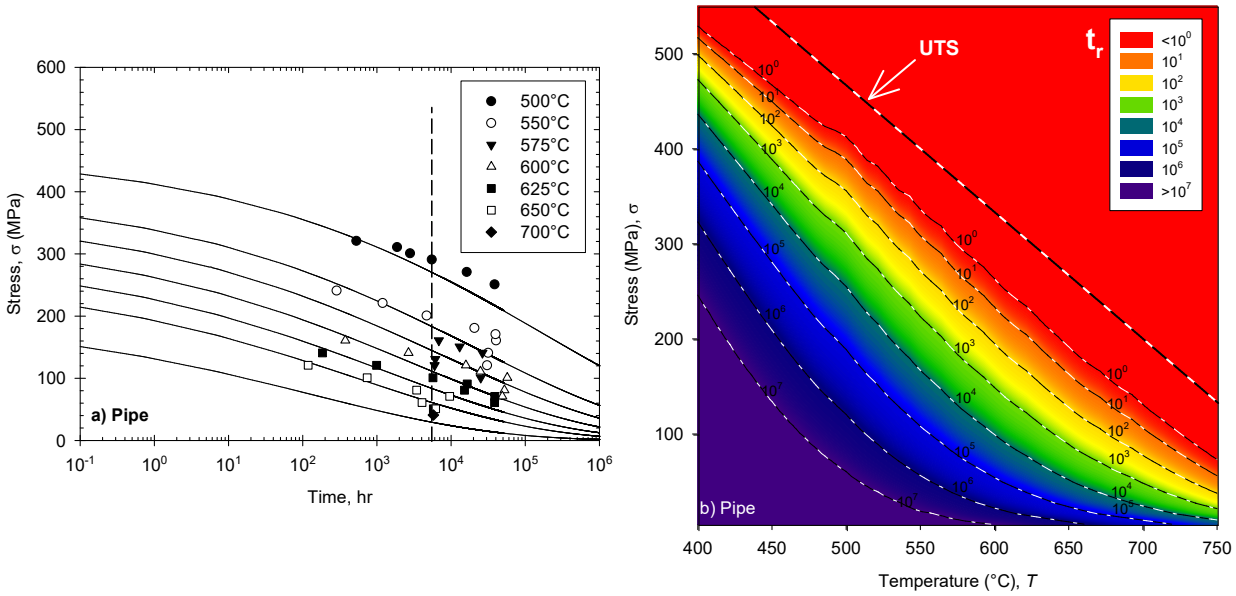

Figure 4.10 - Using Wilshire [Eq. (4.4)] in a pipe a) stress-rupture predictions for alloy P91 and b) design rupture maps are obtained.

It is observed that the Wilshire stress-rupture model successfully extrapolates long-term data not used in the calibration process for all forms because it follows the trend of the experimental data. Despite the model clear trend, the material constants that differ from form to form affects the overall performance of the model. The accuracy of calibration and extrapolation is assessed using the Normalized-Mean Square Error function (NMSE). The NMSE is calculated for each isotherm and the overall in the following form

$$NMSE = \frac{1}{N}\sum_{i=1}^{N}\frac{(X_{sim,i} - X_{\exp,i})^2}{\bar{X}_{sim}\bar{X}_{\exp}} \tag{0.6}$$

where $X_{\exp,i}$ and $X_{sim,i}$ are the experimental and simulated data respectively and $\bar{X}_{\exp}$ and $\bar{X}_{sim}$ are the mean values. The NMSE values for each material form (tube, plate, and pipe) are given in Figure 4.11. It is observed that the plate, represented as the grey line, has the least error therefore has the highest accuracy of the three forms follow by the tube and then the pipe for the overall model and across isotherms as well.

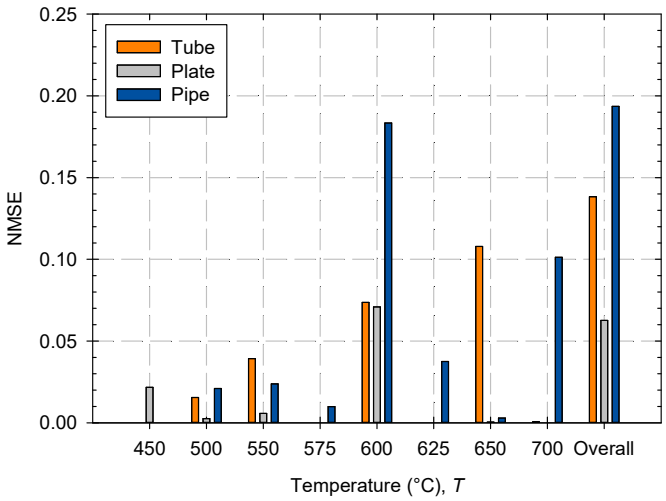

Figure 4.11 - Normalized-Mean Squared Error at each isotherm for the tube, plate, and pipe for stress-rupture [Eq. (4.4)]

4.7 Minimum-Creep-Strain-Rate Prediction Model

Using material constants (Q_c^* , k_2, and v) from Table 4.2 and plugging them into Wilshire [Eq. (4.5)] the MCSR models are obtain illustrated in Figure 4.12 (a), (b), and (c) for tube, plate and pipe. Like the stress-rupture model, the vertical dashed line across the graph represents the data used for the calibration and the extrapolative results. The lowest minimum-creep-strain-rate used for all three forms is $\left(10^{-3}\right)$ where extrapolations are made from high strain levels to lower.

Similarly to the stress-rupture model, it is observed that the Wilshire minimum-creep-strain-rate successfully extrapolates long-term data that is not used in the calibration process. The material constants are different for the three forms. Comparing the performance as well the NMSE values are given for the three material forms as shown in Figure 4.13. Unlike the stress-rupture model, the form with the lowest error for the minimum-creep-strain-rate model is the pipe and is follow by the plate and lastly the tube. The stress-rupture model has less data than the minimum-creep-strain-rate. Both the data sets for the tube and plate almost double in size from the stress-rupture to the minimum-creep-strain-rate but the pipe decreases in size. Stress-rupture has 80 data points for tube and plate and 40 for the pipe and the minimum-creep-strain-rate has 180 data points for the tube, 130 for the plate, and 30 for the pipe. This explains why the pipe in the minimum-creep-strain-rate has the highest accuracy. The less data needed to extrapolate the less error it contains in this situation. The form that had a consistent trend in both models is the tube with the highest error. Because of the limited information from the pipe in both models it is safe to assume that the plate is the best in terms of accuracy relative to the other two forms.

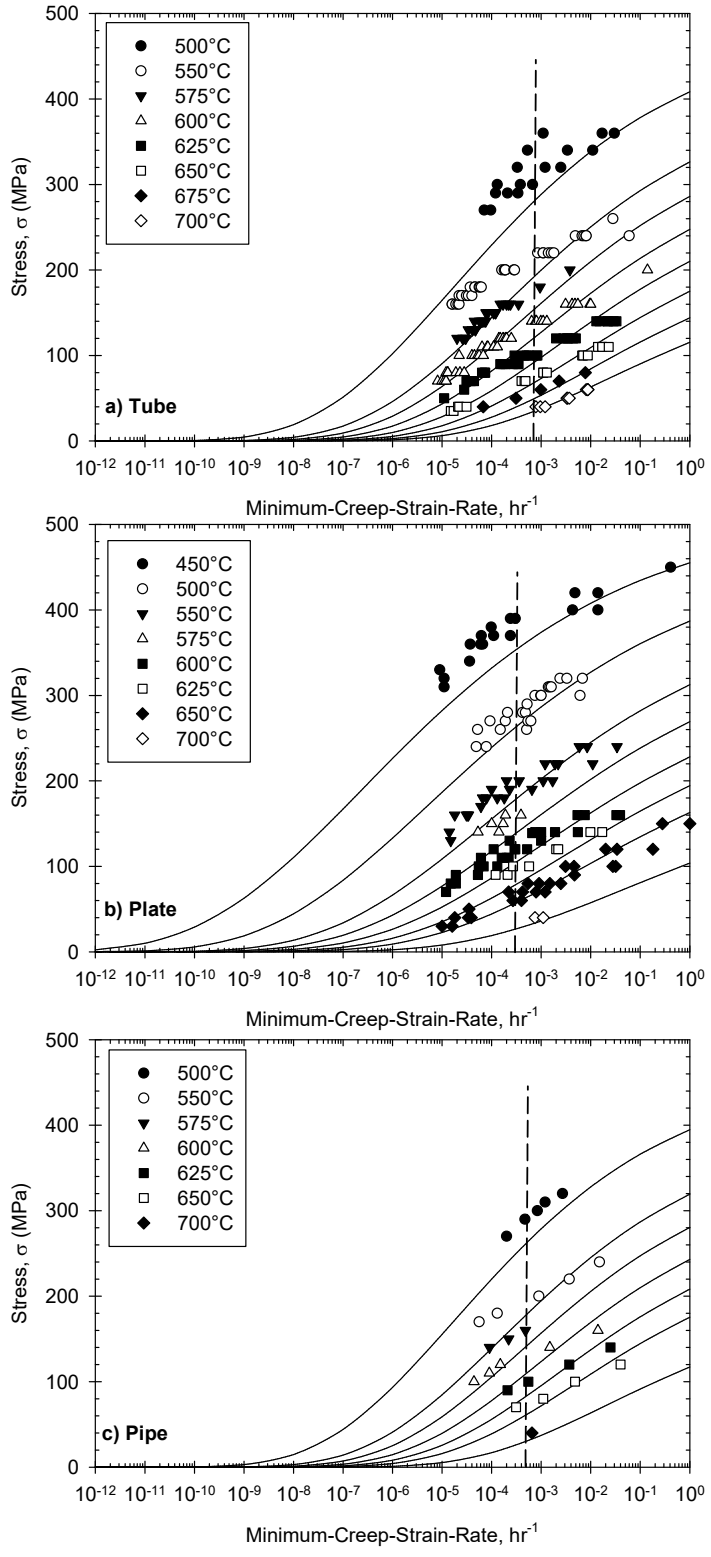

Figure 4.12 - Minimum-creep-strain-rate (MCSR) predictions of Wilshire [Eq. (4.5)] compared to P91 experimental data at multiple isotherms for (a) tube, (b) plate, and (c) pipe

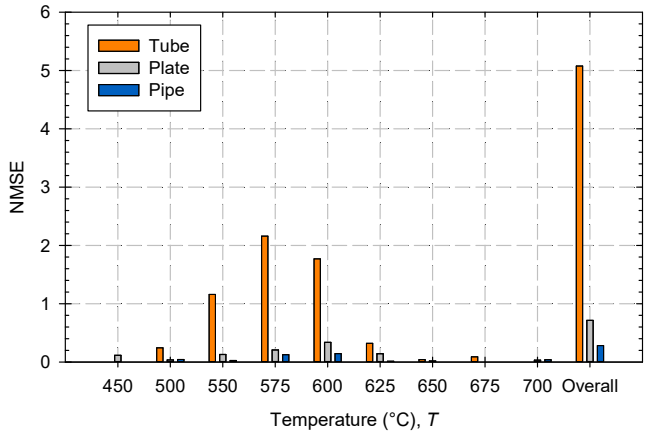

Figure 4.13 - Normalized-Mean Squared Error at each isotherm for the tube, plate, and pipe for minimum-creep-strain rate [Eq. (4.5)]

The models have different performance from form to form because of the variance of material constants. Creep behavior from test to test varies because of defects of the microstructure in the material due to manufacturing. As stated in this study, each form had various heat processes apply to it. The thermomechanical process also differs from tube, plate, and pipe making the material susceptible to additional defects depending on the form. The plate had the best performance overall and is the one with the most significant difference in the chemical composition. Therefore, the chemical composition of the plate and the processes it undergoes makes the plate less exposed to defects and has the best performance against creep.

4.8 Overview

In this Chapter the research objectives were to assess the stress-rupture and minimum-creep-strain-rate prediction models for Wilshire using alloy P91 in tube, plate, and pipe form. As well as provide design maps as tools for design engineers and using the Wilshire stress-rupture equation.

The Wilshire models were calibrated with the existing analytical method. It is discovered that despite the material remains the same for tube, plate, and pipe the material constants are different for each form. During heat and manufacturing processes the chemical composition as well as the microstructure of the material changes. The change of process and chemical composition then affects the material constants obtain from the analytical approach. The plate is the form with the most notably chemical composition change.

Using the material constants obtain for Q_c^*, k_1, and u the stress-rupture Wilshire equation was then calibrated for each of the forms. The model successfully extrapolates the data not used in calibration for all forms. Using the NMSE each of the forms were compared to vet which has the best performance against creep behavior. It is then concluded that the plate has the best performance overall for the stress-rupture model. Using the Wilshire stress-rupture model design maps are created for the tube, plate, and pipe. The maps can be used to make decisions in design depending on the conditions given to engineers. The plate has the most "infinite life" with the largest area for 10^7 implying that the plate also has the best performance for combinations of stress and temperature. Similarly, using the material constants Q_c^*, k_1, and u the MCSR Wilshire model was calibrated for each of the forms. Similarly, to the stress-rupture model the MCSR model successfully extrapolates data. The pipe has the best performance according to the NMSE in such model, but the lack of data provided for the pipe leaves room to analyze before concluding is has the actual best performance. The second one with the best performance and with enough data is the plate.

Overall the plate has the best performance, it sustains a high level of accuracy and has enough data for calibration in both models. Future work in this area of study is to assess the impact different processes have on the performance of the material. Using the well-established Wilshire method, efforts to recreate the full creep curve are also an area of interest in this study.

CHAPTER 5: MODIFIED WILSHIRE MODEL FOR LONG-TERM CREEP DEFORMATION AND DAMAGE PREDICTION

5.1 Introduction

The Wilshire equations were introduced and have been well-accepted for the stress-rupture and MCSR models but there exists a third equation that describes time-to-strain predictions [64-66]. Literature review finds that the Wilshire model produces accurate long-term extrapolations across a wide range of stress and temperature for numerous alloys [60-61,63-66]. Despite Wilshire's well-established equations, the ability to predict creep deformation is limited due to a complex calibration process required to make analytical predictions. In addition, the analytical time-to-strain equation is not compatible with finite element analysis. The Wilshire model needs to be modified to enable the prediction of creep deformation across a wide range of stress and temperature.

The objective of Chapter 5 is to develop a CDM-based Wilshire (WCS) model that can predict long-term creep deformation, damage, and rupture. To accomplish this objective the following steps must be completed. The WCS model is derived; where the Wilshire stress-rupture and MCSR equations are incorporated into the Sinh CDM framework. Creep deformation data is collected for alloy P91 for a single isotherm and multiple stress levels from literature as shown in Figure 3.3. Material constants are obtained for the WCS model using the existing calibration approaches. Creep deformation and damage predictions are compared to experimental to demonstrate the accuracy of the WCS model. A parametric study is performed to assess the interpolation and extrapolation ability of the WCS model.

5.2Wilshire Equations and Previous Approaches

The Wilshire equations are described in [Eq. (4.4)] and [Eq. (4.5)] for predictions of stress-rupture and MCSR. Stress-rupture and MCSR predictions can be rearranged for predictions in the following form

$$t_f = \frac{\left[-\ln\left(\frac{\sigma}{\sigma_{TS}}\right)\Big/ k_1\right]^{\frac{1}{u}}}{\exp\left(-\frac{Q_c^*}{RT}\right)} \tag{5.1}$$

$$\dot{\varepsilon}_{\min} = \frac{\left[-\ln(\frac{\sigma}{\sigma_{TS}})\Big/ k_2\right]^{\frac{1}{v}}}{\exp\left(Q_c^*/RT\right)} \tag{5.2}$$

to obtained desired t_f and $\dot{\varepsilon}_{\min}$ at given stress and temperature. The calibration method has already been discussed and there have been many studies that applied the Wilshire equations.

The Wilshire equations been applied to a variety of alloys including polycrystalline copper, 9-12% chromium steels (Grade 122, 11Cr-2W, and 12Cr stainless steel bars), 1Cr-1Mo-0.25V, 316H stainless steel, among others [61,63-64,67-68]. Note that not all these materials listed were heat treated or post-process as in the study of Grade 122 steels, where the material is in plate and pipe form and has been forged at distinct stresses and temperatures producing multiple material batches [63]. The Wilshire equations has accurate extrapolations for multi-batch short-term stress-rupture data, typically less than 5000 hours, out to 100,000 hours for multiple isotherms [63,65,69,71].

To better predict SR and MCSR across a range of stresses, Wilshire et al introduced the region-splitting approach where the material constants k_1, u, k_2, and v are split into two sets for low and high stress ratios, σ/σ_{TS} respectively [63-66]. Following Wilshire's approach, Cedro et al found that region-splitting at the yield strength minimized the error in rupture predictions of alloys HR6W and Sanicro 25 [72]. When region-splitting is not considered, miscalculation of rupture time predictions arises commonly caused by transitions on the deformation mechanisms [72]. Deformation mechanism maps can be consulted to decide on the split point. Previously in Chapter 4, region-splitting is not considered which carries a major part of the error especially in large datasets. Despite this the Wilshire model makes reasonable predictions across a decade and at multiple isotherms. When properly calibrated, the Wilshire equations predict the stress-rupture and MCSR over a wide range of stress and temperature [67,69].

5.3 Wilshire Time-to-Creep-Strain

Wilshire introduced a third equation for predicting the time-to-creep-strain, t_ε as follows

$$\frac{\sigma}{\sigma_{TS}} = \exp\left(-k_3\left[t_\varepsilon \exp\left(-\frac{Q_c^*}{RT}\right)\right]^w\right) \tag{5.3}$$

where k_3 and w are material constants at a constant creep strain, ε_{cr} [65,69]. To calibrate the model, the creep deformation data of many experiments is converted into a tabular form where the stress, temperature, and time-to-creep-strain (σ, T, t_ε) are reported with respect to creep strain, ε_{cr} e.g. 0.01%, 0.05%, 0.1%, 0.2%, 0.5%, 1%, 5%, creep ductility). For each creep strain, ε_{cr} in the table, an independent set of k_3 and w constants must be determined. The k_3 and w material constants are obtained by plotting the experimental $\ln\left[-\ln\left(\sigma/\sigma_{TS}\right)\right]$ versus

$\ln\left[t_\varepsilon \exp\left(-Q_c^*/RT\right)\right]$ where the slope is w and the y-intercept is the k_3 constant. Region splitting may be required where the k_3 and w constants specific to each creep strain, ε_{cr} are different in low- and high-stress regions [65-66].

Creep deformation predictions can be made by expressing the k_3 and w constants as a function of creep strain,

$$k_3 = f_1(\varepsilon_{cr}) \tag{5.4}$$

$$w = f_2(\varepsilon_{cr}) \tag{5.5}$$

where typically, a single of w is chosen to represent all creep strains and k_3 takes a power-law form

$$k_3 = k_{3,0} + k_{3,1}\left(\varepsilon_{cr}\right)^{k_{3,2}} \tag{5.6}$$

where $k_{3,0}, k_{3,1}$, and $k_{3,2}$ are additional material constants [69,73-74]. Introducing [Eq. (5.4)-(5.5)] into [Eq. (5.3)] furnishes the following

$$\frac{\sigma}{\sigma_{TS}} = \exp\left(-f_1(\varepsilon)\left[t_\varepsilon \exp\left(-\frac{Q_c^*}{RT}\right)\right]^{f_2(\varepsilon)}\right) \tag{5.7}$$

where the time-to-creep-strain, t_ε and the creep strain, ε_{cr} exist together. Creep deformation is predicted by rearranging [Eq. (5.7)] to furnish a complex creep deformation $\varepsilon_{cr} = f\left(\sigma, \mathrm{T}, t\right)$ equation. Note, if k_3 and w exist as functions of creep strain [Eq. (5.4)-(5.5)], an exact solution to $\varepsilon_{cr} = f\left(\sigma, \mathrm{T}, t\right)$ does not exist and a numerical solver must be employed.

Harrison assessed the time-to-strain approach to predict creep deformation prediction for alloy 720Li [74]. Region-splitting was employed using $0.65\,\sigma/\sigma_{TS}$ as a split point, where it is assumed that dislocations within the grain boundaries occurred. Using [Eq. (5.6)] to obtained material constants, creep deformation predictions are made across three combinations of stress and temperatures. Predictions were made for less than 3000 hours, and it is concluded that it extrapolates accurately introducing the functional form [Eq. (5.6)] to the existing model. Although Harrison concludes this, the method depends on ε_{cr}, which is unknown, and there is still not clarity on how to choose the time to creep strain. Evans also studied the time-to-strain approach in Waspaloy. The study normalize creep strain by ductility using $\varepsilon^{*} = \varepsilon/\varepsilon_{f}$, to avoid the issue that at some t_{ε} values, which there little clarity on how to choose the values, some specimens have already failed. Although efforts were made to avoid this issue, the results obtained a consistent over prediction in the time for failure as well as in the creep strain curves [75]. There seems to be a variety of complications in using the time-to-strain equation to predict creep deformation and little consistency on the methods of implementation.

5.4 Sin-Hyperbolic CDM Model

The sin-hyperbolic (Sinh) model is a modern continuum damage mechanics (CDM)-based model for creep deformation and damage prediction [76-79]. The creep-strain-rate takes the following form

$$\dot{\varepsilon}_{cr} = A \sinh\left(\frac{\sigma}{\sigma_{s}}\right) \exp\left(\lambda \omega^{3/2}\right) \tag{5.8}$$

where A and σ_{s} are the MCSR constants and ω is damage ranging from $0 < \omega < 1$. The constant λ is defined as

$$\lambda = \ln\left(\dot{\varepsilon}_{final} / \dot{\varepsilon}_{\min}\right) \tag{5.9}$$

where the MCSR, $\dot{\varepsilon}_{\min}$ and final-creep-strain-rate, $\dot{\varepsilon}_{final}$ are measured from experimental data. The MCSR arises in [Eq. (5.8)] when damage is zero

$$\dot{\varepsilon}_{\min} = A \sinh\left(\frac{\sigma}{\sigma_s}\right) \tag{5.10}$$

where temperature-dependence is not explicit. Damage evolution takes the following form

$$\dot{\omega} = \frac{\left[1-\exp(-\phi)\right]}{\phi} M \sinh\left(\frac{\sigma}{\sigma_t}\right)^{\chi} \exp\left(\phi\omega\right) \tag{5.11}$$

where the M, χ and σ_t are the rupture prediction material constants that are analytically determined from stress-rupture data, ϕ is the damage trajectory material constant determine via numerical optimization of the creep deformation, and ω is damage. Integration of damage evolution [Eq. (5.11)] from $0 < t < t_f$ and $0 < \omega < 1$, furnishes rupture prediction as

$$t_f = \left[M \sinh\left(\frac{\sigma}{\sigma_t}\right)^{\chi} \right]^{-1} \tag{5.12}$$

where temperature-dependence is not explicit. Integration of damage evolution [Eq. (5.11)] from $0 < t < t_f$ and $0 < \omega < \omega$, furnishes damage as

$$\omega(t) = -\frac{1}{\phi} \ln\left[1 - \left[1-\exp(-\phi)\right] \frac{t}{t_f} \right] \tag{5.13}$$

where the material constants remain the same.

The Sinh model has been applied to model the creep behavior of 304 stainless steel, Waspaloy, and Hastealloy X [76-78]. The Sinh model was designed to exhibit less stress-sensitive,

less mesh-dependent, and better convergence when compared to classic CDM creep laws [40,79]. In the Sinh model, critical damage is always equal unity, $\omega = 1$ irrespective to loading conditions (uniaxial or multiaxial). The model has been implemented in commercial FEA software to simulate multiaxial creep including notches and cracks [77,79]. In addition, a method for calibrating the Sinh model using data from disparate sources has been developed [6].

5.5 Problem with Wilshire and Sinh CDM Model

The stress-rupture, MCSR, and creep deformation predictions of Wilshire and Sinh models are examined closely. Regarding Wilshire,

- the stress-rupture and MCSR predictions [Eq. (5.1)-(5.2)] include temperature-dependence, can be calibrated analytically, and are accurate over a wide range of temperature and stress.
- the calibration process for creep deformation prediction [Eq. (5.3)] is complicated and tedious. A large database of creep deformation data is needed. Tables of time-to-strain [Eq. (5.3)] for each creep strain, ε_{cr} of interest must be generated and a set of k_3 and w constants calibrated. The k_3 and w constants are then regressed into a function of creep strain. Depending on the k_3 and w functions, a closed and differentiable creep deformation equation may not exist. If a closed-form does not exist, additional iterations are required at all material integration points of the elements, every time step, in a finite element problem. Subsequently, the Wilshire time-to-strain [Eq. (5.3)] has slower convergence rates in finite element analysis when compared to other creep models.

Regarding Sinh,

- the Sinh model has been demonstrated to predict the creep deformation of a variety of alloys, with less stress-sensitivity, less mesh-dependence, and better convergence rates than conventional creep models.
- temperature-dependence is not stated explicitly in the Sinh model such that there exists a challenge in calibrating and validating the model for non-isothermal conditions.

Overall, both the Wilshire equations and Sinh model need further development. It is hypothesized that the Wilshire model can be integrated into Sinh CDM framework to derive a new model that produces accurate long-term creep deformation and damage predictions across a wide range of temperature and stress.

5.6 CDM-Based Wilshire Model (WCS)

The new CDM-based Wilshire model consists of a set of coupled differential equation for creep-strain-rate and damage evolution. For brevity, the model is referred to as the WCS model. The creep-strain-rate is furnished by taking the Sinh creep-strain-rate [Eq. (5.8)] and replacing the Sinh MCSR [Eq. (5.10)] with Wilshire's [Eq. (5.2)] as follows

$$\dot{\varepsilon}_{cr} = \frac{\left[-\ln\left(\frac{\sigma}{\sigma_{TS}}\right) \Big/ k_2\right]^{\frac{1}{v}}}{\exp\left(Q_c^* / RT\right)} \exp\left(\lambda\omega\right) \tag{5.14}$$

where ω is raised to the power of 1 in this modified form, which allows a closed form solution to be obtained suitable for FEA with faster convergence rate. The damage evolution is furnished by taking the Sinh damage evolution [Eq. (5.11)] and replacing the Sinh rupture prediction [Eq. (5.12)] with Wilshire's [Eq. (5.1)] as follows

$$\dot{\omega} = \frac{\left[1-\exp(-\phi)\right]}{\phi} \frac{\exp\left(-\frac{Q_c^*}{RT}\right)}{\left[-\ln\left(\frac{\sigma}{\sigma_{TS}}\right)\Big/ k_1\right]^{\frac{1}{u}}} \exp\left(\phi\omega\right) \tag{5.15}$$

The damage [Eq. (5.13)] is preserved. The complete WCS model is summarized in Table 5.1. The Wilshire material constants $\left(\sigma_{TS}, Q, k_1, u, k_2, v\right)$ and Sinh material constants $\left(\lambda, \phi\right)$ can be determined using the existing calibration approach for each model respectively [63-66,76-79]. Any Wilshire or Sinh constants that have been previously calibrated for a given material can be directly applied in the new model.

Table 5.1 - Summary of WCS Model

Feature	Equation	Origin	Material Constants
MCSR	[Eq. (5.2)]	Wilshire	σ_{TS}, Q, k_2, v
Rupture	[Eq. (5.1)]	Wilshire	σ_{TS}, Q, k_1, u
Creep-strain-rate	[Eq. (5.14)]	Combined	$\sigma_{TS}, Q, k_2, v, \lambda$
Damage evolution	[Eq. (5.15)]	Combined	$\sigma_{TS}, Q, k_1, u, \phi$
Damage	[Eq. (5.13)]	Sinh	ϕ

5.7 Material Constants

The material constants Wilshire and Sinh must be calibrated. In the Wilshire equations, the material constants k_1 and u from [Eq. (5.1)] and k_2 and v from [Eq. (5.2)] are calibrated using region splitting as shown in Figure 5.1 (a) and (b) respectively. Consulting the deformation mechanism map for alloy P91 shown in Figure 2.4 it is determined that region-splitting is required as a mechanism transition between power-law and viscous creep occurs at values >110 MPa at 600°C [16]. Discussed in Chapter 4 and presented in Table 3.3 it is determined that σ_{TS} at 600°C

is approximately 357 MPa and the activation energy for P91 in tube form is $Q_c^* \cong 230\ kJmol^{-1}$ [53]. Subsequently, region splitting occurs at a stress ratio σ/σ_{TS} of 0.31 approximately.

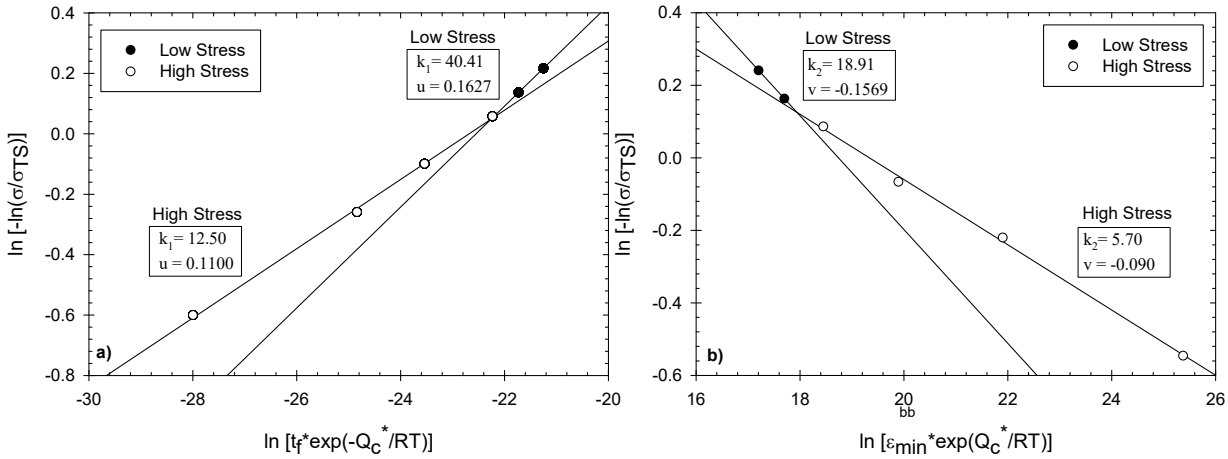

Figure 5.1 – Normalized (a) stress-rupture and (b) minimum-creep-strain-rate (MCSR) data of P91 at 600°C for the calibration of k_1, u and k_2, v respectively with region splitting at a stress ratio of 0.31.

The calibrated material constants Q_c^*, k_1, u, k_2, and v are summarized in Table 5.2. The material constants correspond to previous studies and show the expected trend in which at high σ/σ_{TS} the material constants are usually lower than those obtained at low σ/σ_{TS} [63-66,72].

Table 5.2 – Summary of Wilshire material constants for P91 tube at 600°C with region splitting at a stress ratio of $\sigma/\sigma_{TS} = 0.31$

Region	Q_c^*	k_1	u	k_2	v
σ/σ_{TS}	$kJmol^{-1}$	hr^{-u}		hr^{v}	
Low	230	40.41	0.1627	18.91	-0.1569
(High)	(--)	(12.50)	(0.1100)	(5.70)	(-0.090)

In the Sinh model, the material constants λ and ϕ are required. The λ constant is obtained through [Eq. (5.9)] analytically using creep-strain-rate data. The ϕ constant is obtained

numerically, by optimizing [Eq. (5.8)] and [Eq. (5.13)] with creep deformation data. The ϕ constant is obtained numerically, by optimizing [Eq. (5.8)] and [Eq. (5.13)] with creep deformation data. The objective function is the NMSE presented in [Eq. (0.6)]. To obtain the ϕ constant, the Q_c^*, k_1, u, k_2, v and λ are required. The calibrated λ and ϕ material constants are provided in Table 5.3.

Table 5.3 – Summary of the individually calibrated Sinh material constants λ and ϕ

Temperature, T (°C)	Stress, σ (MPa)	$\dot{\varepsilon}_{final}$ (hr^{-1})	$\dot{\varepsilon}_{\min}$ (hr^{-1})	λ	ϕ	NMSE
600	100	$1.26(10^{-4})$	$5.12(10^{-7})$	5.51	5.16	$2.79(10^{0})$
600	110	$1.60(10^{-4})$	$8.42(10^{-7})$	5.25	3.74	$6.69(10^{0})$
600	120	$2.64(10^{-4})$	$1.78(10^{-6})$	5.00	3.22	$1.92(10^{-5})$
600	140	$5.77(10^{-4})$	$7.57(10^{-6})$	4.33	2.51	$3.00(10^{1})$
600	160	$2.55(10^{-3})$	$5.64(10^{-5})$	3.81	1.45	$1.16(10^{2})$
600	200	$6.48(10^{-2})$	$1.81(10^{-3})$	3.56	4.14	$1.06(10^{-5})$

During calibration, it was determined that a single set of λ and ϕ do not exist for all experiments; therefore, λ and ϕ were calibrated individual for each creep curve. Past studies have shown that these constants also exhibit temperature-dependence [6,40,76-79]. To account for the co-dependence on stress and temperature, regression is performed, where a modified Eyring equation is employed for λ and ϕ as follows

$$\lambda = \lambda_0 \exp\left(\frac{-V_\lambda^* \sigma}{k_b T}\right) \tag{5.16}$$

$$\phi = \phi_0 \exp\left(\frac{-V_\phi^* \sigma}{k_b T}\right) + 1 \tag{5.17}$$

where V_λ^* and V_ϕ^* are the activation volumes (or stress coefficient) corresponding to λ and ϕ, k_b is the Boltzmann constant $1.3806\left(10^{-23}\right)\ J/K$, and λ_0, ϕ_0 are material constants [80-81]. In the ϕ [Eq. (5.17)], the +1 term is added so that $\phi \geq 1$ always for numerical reasons [76-79].

Using this two new models [Eq. (5.16)] and [Eq. (5.17)] the stress and temperature dependence issue that the Sinh has is now resolve. Using the optimal λ and ϕ values, the activation volumes and λ_0, ϕ_0 are found and are summarized in Table 5.4. The predictions and the fitting of [Eq. (5.16)] and [Eq. (5.17)] are shown in Figure 5.2, where it is observed that the model crosses the data and there is a small error on some of the optimal values. Due to the numerical nature of both material constants, λ and ϕ, even though the solutions are not optimal, a small change would have little impact on the overall model; as an exchange realistic results across isotherms and stresses can be obtained.

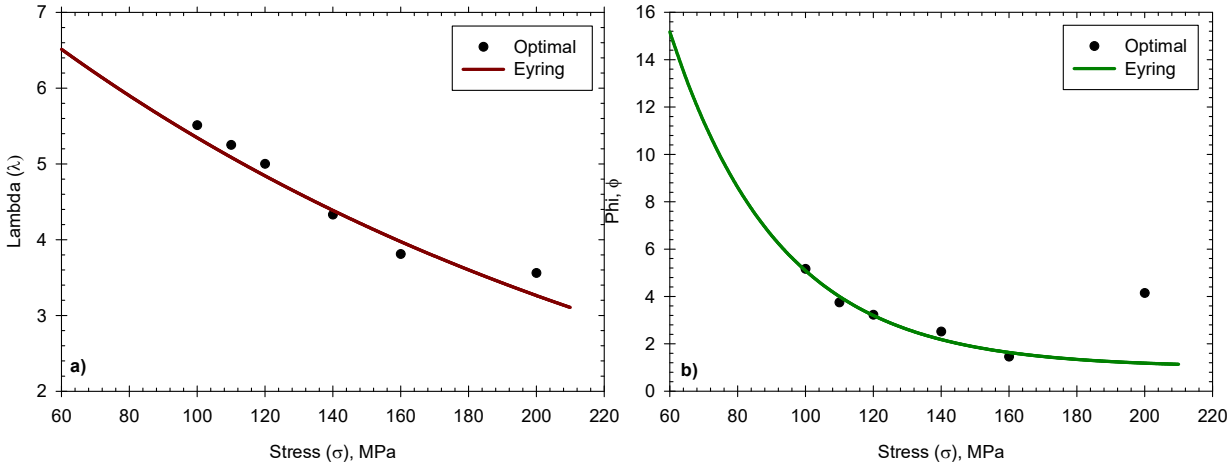

Figure 5.2 – Regressed (a) λ and (b) ϕ material constants using [Eq. (5.16)] and [Eq. (5.17)] respectively plotted against their individual calibrated values.

Table 5.4 – Summary of material constants for modified Eyring [Eq. (5.16)-(5.17)].

Eyring [Eq. (5.16)]		Eyring [Eq. (5.17)]	
Material Constants	Values	Material Constants	Values
λ_0 (unitless)	8.76	ϕ_0 (unitless)	91.5
$V_\lambda^*\,(cm^3)$	$5.95\left(10^{-23}\right)$	$V_\phi^*\,(cm^3)$	$3.75\left(10^{-22}\right)$
$k_b\,(J/K)$	$1.3806\left(10^{-23}\right)$	$k_b\,(J/K)$	$1.3806\left(10^{-23}\right)$
Temperature (K)	873.15	Temperature (K)	873.15

A behavior observed in the optimal values of both λ and ϕ in Figure 5.2 (a) and (b) is that typically as stress increases, λ and ϕ decrease. This behavior is expected, as materials have longer lifetimes creep deformation curves become almost a flat line with less creep ductility. Recalling [Eq. (5.9)], it is noticeable that as $\dot{\varepsilon}_{final}$ approaches $\dot{\varepsilon}_{\min}$ then $\lambda \to 0$. Therefore, a long-term creep curve is associated with a small λ value and for a short-term creep curve λ is larger. To further apply the WCS model to a FEA software parametric simulations are shown in Figure 5.3 for (a) λ and (b) ϕ at distinct combinations of stress and temperatures to prove the model captures the expected trend. As observed, the expected behavior is perfectly described by the model also in agreement to the trend seen in Figure 5.2. The model physically represents the proper behavior across multiple stresses and temperatures. A summary of the new λ and ϕ values using [Eq. (5.16)-(5.17)] is shown in Table 5.5 with the updated NMSE values. Notice the NMSE values did not change dramatically on most stress levels.

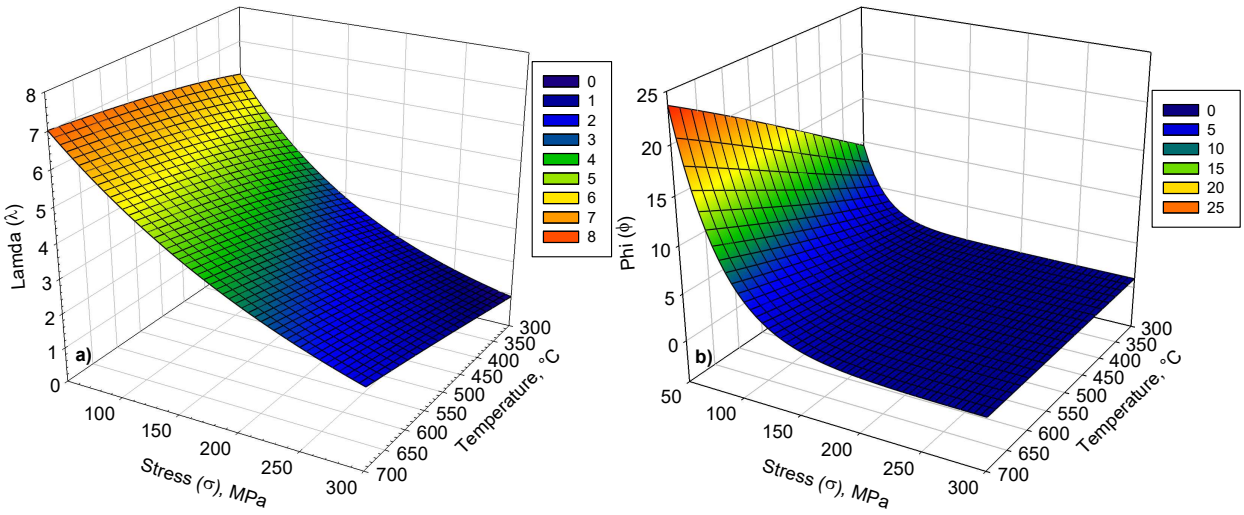

Figure 5.3 – Parametric simulation of (a) λ and (b) ϕ at distinct combinations of stresses and temperatures.

Table 5.5 – Summary of λ and ϕ values using [Eq. (5.16)-(5.17)]

Temperature, T (°C)	Stress, σ (MPa)	λ	ϕ	NMSE
600	100	5.35	5.09	$2.84(10^{0})$
600	110	5.09	4.00	$9.23(10^{0})$
600	120	4.84	3.20	$3.05(10^{-3})$
600	140	4.39	2.18	$3.25(10^{1})$
600	160	3.98	1.63	$1.18(10^{2})$
600	200	3.26	1.18	$1.17(10^{1})$

5.8 Creep Deformation and Damage Predictions

Creep predictions are made using the calibrated material constants in Table 5.2 and Table 5.5 respectively. The stress-rupture and MCSR predictions are made using [Eq. (5.1)-(5.2)] respectively and are illustrated in Figure 5.4. The predictions for stress-rupture and MCSR are accurate with the single isotherm using region-splitting. The experimental and simulated rupture times are compared in Table 5.6 with the percent error between predictions. Using a + and – sign

shows that the model is over and underpredicting respectively. The model is conservative for most of the stress levels and in the ones that is over predicting the percent error is not a major concern. The MCSR predictions are accurate which facilitates the overall creep deformation predictions.

Table 5.6 – Experimental and simulated rupture time from the damage model and the Wilshire rupture predictions with percent error.

Stress, σ (MPa)	Actual Rupture Time (hr)	Simulated Rupture Time (hr)	Percent Error %
100	34,121.41	34,014.31 (-)	0.31
110	21,147.22	21,079.44 (-)	0.32
120	12,796.49	13,533.69 (+)	5.76
140	3,460.80	3,384.98 (-)	2.19
160	943.46	835.44 (-)	11.45
200	40.13	43.22 (+)	7.71

*+ and – are for over and underpredictions respectively.

Creep deformation predictions using [Eq. (5.14)] are shown in Figure 5.5 (a) on a logarithmic time scale. It is observed that the novel constitutive model accurately fits for the secondary and tertiary creep regimes creep regimes. Damage predictions, using the integral form of [Eq. (5.15)], are provided in Figure 5.5 (b) on a logarithmic time scale. In all cases, the critical damage is found to be $\omega = 1$ at rupture.

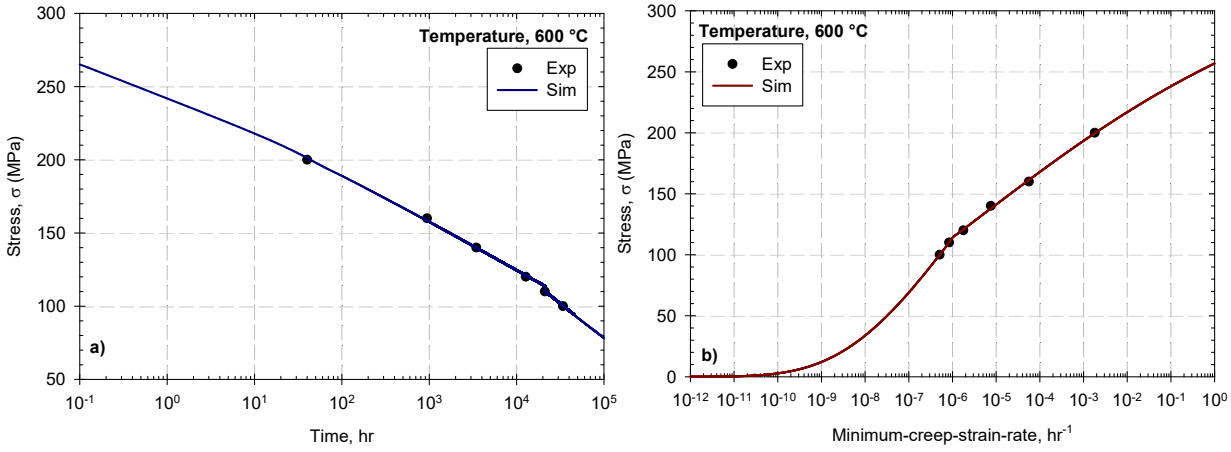

Figure 5.4 - WCS model predictions of (a) stress-rupture and (b) minimum-creep-strain-rate (MCSR) data. Note that the x-axis in both scenarios are in logarithmic scale.

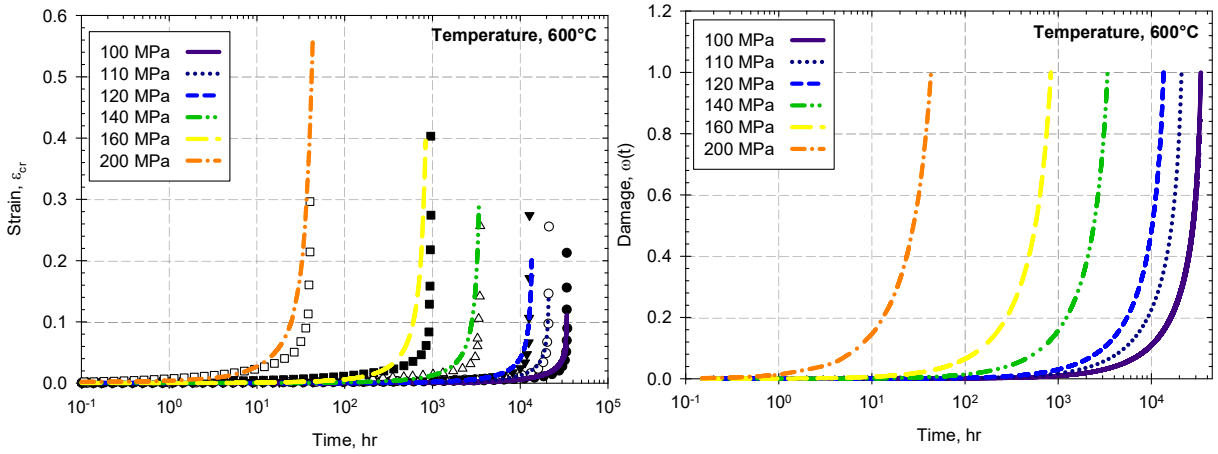

Figure 5.5 – WCS model predictions of (a) creep deformation [Eq. (5.14)] and (b) damage [Eq. (5.13)] for alloy 91 at 600 °C subject to 100, 110, 120, 140,160, and 200 MPa. Time is on a logarithmic scale.

Overall the model fits accurately the creep deformation curves and predict rupture time with a small percent error. The explicit stress and temperature dependency allow a clear analytical approach to obtained creep deformation and damage evolution predictions. Also the differential form in which both creep strain [Eq. (5.14)] and the damage rate [Eq. (5.15)] are presented allows

FEA software to be used to predict creep behaviors as well. A closed-form solution for creep strain is introduced as well, which is convenient for FEA convergence. The model is conservative.

5.9 Parametric Exercise of WCS Model

Parametric simulations are performed using various combinations of stress and temperature to the constitutive WCS model. Extreme condition tests are performed to vet the accuracy of predictions where data is not given, especially for future FEA simulations.

These tests are separated into stress and temperature tests in which the stress-rupture, MCSR, and creep ductility are analyzed shown in Table 5.7. Due to the way [Eq. (5.1)-(5.2)] are presented, when temperature and stress are 0 then the equation becomes undefine. The stress test includes zero stress, yield stress, and UTS and the temperature test are absolute zero, room temperature, and near melting temperature. Additionally, typical operating conditions on an advance Ultrasupercritical (A-USC) power plant are given. There seems to be coherency in the way the model behaves at extreme conditions in which realistic results are given.

Table 5.7 – Extreme stress and temperature test for WCS model using rupture time, MCSR, and creep strain

Test	**Stress Test (** MPa **)** (at $873\ K$)			**Temperature Test (** K **)** (at $160\ MPa$)			**A-USC (** MPa, K **)**
Type	Zero Stress	Yield Stress	UT Stress	Absolute Zero	Room Temperature	Melting Temperature	Operating Conditions
Value	0	289	357	0	298	1673	34.5 ,1033
t_f (hr)	Undefine	$4.50\left(10^{-3}\right)$	0	Undefine	$3.00\left(10^{29}\right)$	$2.19\left(10^{-4}\right)$	$9.67\left(10^{4}\right)$
$\dot{\varepsilon}_{\min}$ (hr^{-1})	Undefine	$4.76\left(10^{-2}\right)$	Undefine	Undefine	$2.69\left(10^{-32}\right)$	$3.67\left(10^{1}\right)$	$1.49\left(10^{-6}\right)$
ε_{cr}	Undefine	$5.05\left(10^{0}\right)$	Undefine	Undefine	$9.90\left(10^{-2}\right)$	$1.38\left(10^{1}\right)$	$9.44\left(10^{1}\right)$

Together with the extreme test exercises, parametric studies variating stress and temperature are shown in Figure 5.6. In the temperature variations, Figure 5.6 a), constant stress of 160 MPa is considered for all scenarios. Notice that if such stress level is considered, then from the region-splitting approach, this scenario is operating in high stress except for $500^{\circ}C$ and $525^{\circ}C$. The temperature variations show a consistent behavior when interpolations and extrapolations are performed. Similarly in stress variations at constant temperature, Figure 5.6 b), the predictions are consistent in between and outside the stress levels from the experimental data. It can be clearly observed that as the creep deformation curve tends to longer rupture times creep ductility becomes smaller which is expected from conventional creep curves. Another parametric study is the variation of both stress and temperature as illustrated in Figure 5.7 a). A similar trend is observed in which at higher stress and temperature combinations, creep ductility is larger and vice versa, as stress and temperature are lower, then creep ductility is smaller. Additionally, there is another parametric simulation considering the typical operating conditions from supercritical (SC), ultra-supercritical (USC), and Advance ultra-supercritical (A-USC) powerplants shown in Figure 5.7 b). The operating conditions for the powerplants are obtained from previous studies and is summarized in Table 5.8 [82]. The vertical dotted line, defined as the service life requirement, in in Figure 5.7 b) is the expected life for most materials that operate at these conditions. It is observed that the predicted rupture time for the A-USC does not meet these conditions. There are multiple reasons why this behavior is presented, it can be uncertainty on the data used for calibration or the material selected is not suitable to operate at such conditions. Many materials for A-USC have shorter service life depending on the specifications.

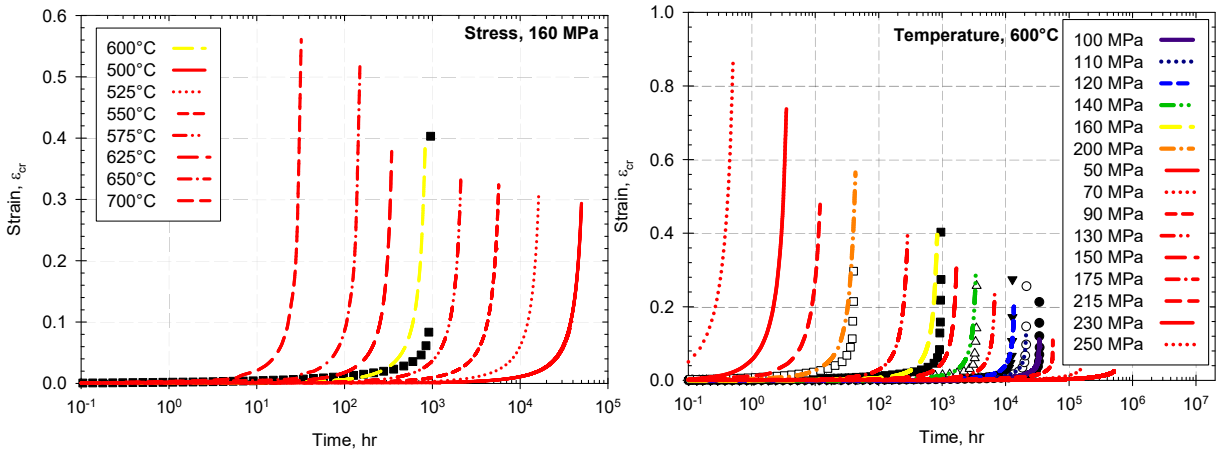

Figure 5.6 – WCS model parametric simulations for both (a) temperature variations and (b) stress variations. Note the x-axis are in logarithmic scale.

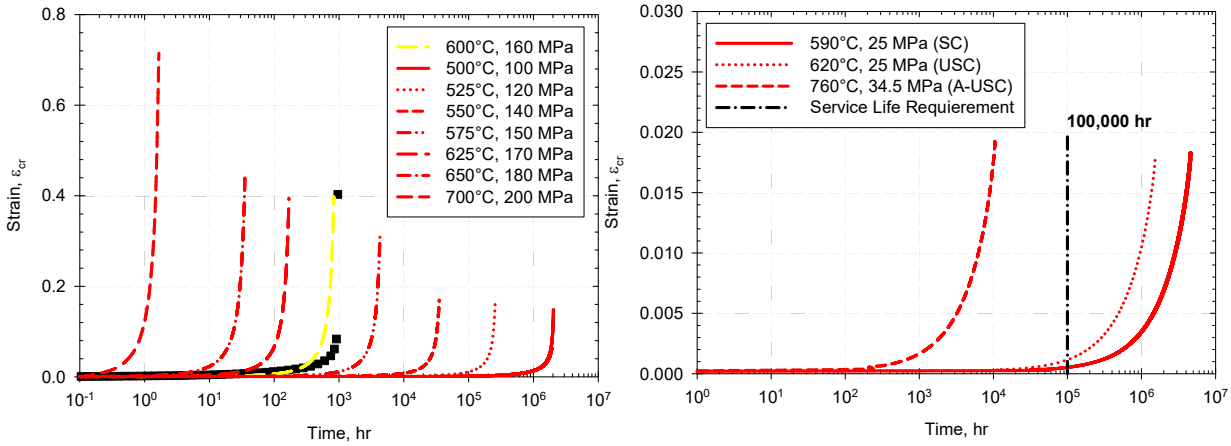

Figure 5.7 – WCS model parametric simulations for (a) both stress and temperature variations and (b) typical operating conditions for conventional supercritical (SC), ultra-supercritical (USC), and advance ultra-supercritical (A-USC) power plants.

Table 5.8 – Conventional operating conditions for supercritical (SC), ultra-supercritical (USC), and Advance ultra-supercritical (A-USC) powerplants [82].

	SC	**USC**	**A-USC**
Temperature, $^{\circ}C$	590	590-620	700-760
Stress, *MPa*	25	25	34.5

Overall WCS model performs in a realistic way which tells the reader that it can be useful for different applications and particularly those mention for SC, USC, and A-USC. The WCS model produces realistic results even where data is not given, making the model reliable for long-term creep deformation predictions, damage evolution predictions, damage rate, rupture time, MCSR, and with a differential form useful for future FEA simulations.

CHAPTER 6: CONCLUSION AND FUTURE WORK

6.1 Conclusions

The objective of this work, the development of a WCS model using the Sinh CDM model has been completed. The capabilities of this new constitutive model are the ability to predict long-term creep deformation, damage rate, damage evolution, rupture time, MCSR, and has explicit stress and temperature gradients.

- The WCS model has proven to fit and predict long-term creep deformation for a wide time period even where data is not provided. The model has an explicit stress and temperature dependency which allows multiple isotherms and stresses to be predicted. Only two additional material constants are necessary to complete the calibration process from the already established and well-accepted Wilshire laws.
- The WCS model predicts both damage evolution and damage rate. Using the rupture predictions from Wilshire the damage accurately represents failure in the material reaching unity close to the rupture time. There seems to be small error from the damage predictions to the actual failure time.
- The WCS model has conserved all Wilshire law properties including the ability to predict rupture time and MCSR as well as the Sinh model capabilities of predicting damage. Introducing the new stress dependent functions to the λ and ϕ Sinh material constants addresses the issue the model has continuously had.

6.2 Future Work

Future work in this area of study is to apply the model using probabilistic to avoid the uncertainty that conventional creep data has. There seems to be little consistency in creep data

where if the same conditions are applied to a specimen, it results in different creep deformation curves. These issues produce a variation of material constants resulting in over and underpredictions of failure time and damage. Adding a probabilistic model would result in better creep deformation and damage predictions. The model must be programed into an FEA software as well to vet the accuracy of simulation predictions. This would allow multiple materials to be calibrated to the model easier as well as more stress and temperature variations. Lastly, the possibility of adding a primary creep model to the WCS model would allow better predictions for materials that are not as creep resistant as P91.

REFERENCES

[1] Haque, M. S. (2018). An Adaptive Creep Modeling Approach Using Metamodeling. The University of Texas at El Paso.

[2] Kassner, M. E., & Smith, K. (2014). Low temperature creep plasticity. Journal of materials research and technology, 3(3), 280-288.

[3] Meher-Homji, C. B., & Gabriles, G. (1998). Gas Turbine Blade Failures-Causes, Avoidance, And Troubleshooting. In Proceedings of the 27th turbomachinery symposium. Texas A&M University. Turbomachinery Laboratories.

[4] Cuzzillo, B. R., & Fulton, L. K. (2014). Failure Analysis Case Studies. Retrieved October 27, 2019, from http://www.berkeleyrc.com/FAcasestudies.html#top.

[5] Janawitz, J., Masso, J., & Childs, C. (2015). Heavy-duty gas turbine operating and maintenance considerations. GER: Atlanta, GA, USA.

[6] Haque, M.S, and Stewart, C. M., 2018, "The Disparate Data Problem: The Calibration of Creep Laws Across Test Type and Stress, Temperature, and Time Scales," Theoretical and Applied Fracture Mechanics, (under review). TAFMEC_2018_166

[7] Haque, M. S., and Stewart, C. M., 2016, "Exploiting Functional Relationships between MPC Omega, Theta, and Sinh-Hyperbolic Models" ASME PVP 2016, PVP2016-63089, Vancouver, BC, Canada, July 17-21, 2016.

[8] Sawada, K., Tabuchi, M., & Kimura, K. (2009). Analysis of long-term creep curves by constitutive equations. Materials Science and Engineering: A, 510, 190-194.

[9] Kraus, H. (1980). Creep analysis. Research supported by the Welding Research Council. New York, Wiley-Interscience, 1980. 263 p.

[10] Evans, H. E. (1984). Mechanisms of creep fracture. Elsevier Applied Science Publishers Ltd., 1984,, 319.

[11] Meyers, M. A., & Chawla, K. K. (2008). Mechanical behavior of materials. Cambridge university press.

[12] Lemaitre, J., Chaboche. 1985. J.L. Mechanics of Solid Materials. Paris: Cambridge University Press.

[13] Betten, J. (2008). *Creep mechanics*. Springer Science & Business Media.

[14] Stewart, C. (2013). A Hybrid Constitutive Model for Creep, Fatigue, and Creep-Fatigue Damage.

[15] Frost, H. J., & Ashby, M. F. (1982). Deformation mechanism maps: the plasticity and creep of metals and ceramics. Pergamon press.

[16] Gorash, Y. (2008). Development of a creep-damage model for non-isothermal long-term strength analysis of high-temperature components operating in a wide stress range.

[17] Chokshi, A. H. (1996). An analysis of creep deformation in nanocrystalline materials. Scripta materialia, 34(12), 1905-1910.

[18] Mesarovic, S. D. (2017). Dislocation creep: climb and glide in the lattice continuum. Crystals, 7(8), 243.

[19] Norton, Frederick Harwood. The Creep of Steel at High Temperature. McGraw-Hill Book Company Incorporated. New York .(1929)

[20] Vega, R, & Stewart, C.M (2019). Development And Application Of Minimum Creep Strain Rate Metamodeling ASME Turbo Expo 2019: Turbomachinery Technical Conference and Exposition Phoenix, Arizona.

[21] Nádai, Arpád, and Arthur M. Wahl. Plasticity. McGraw-Hill Book Company, inc., 1931.

[22] Soderberg, C. R. (1936). The Interpretation of Creep Tests for Machine Design. Trans. ASME, 58(8): 733-743.
[23] McVetty, P. G. (1943). Creep of Metals at Elevated Temperatures-The Hyperbolic Sine Relation between Stress and Creep Rate. Trans. ASME, 65: 761.
[24] Dorn, J. E. (1962). Progress in Understanding High-Temperature Creep, H. W. Gillet Mem. Lecture. Philadelphia: ASTM.
[25] Penny, R. K., and Marriott, D. L., 1995, Design for Creep, Springer, pp.11.
[26] Garofalo, F. (1965). Fundamental of Creep and Creep Rupture in Metals. New York: Macmillan.
[27] Ruano, O. A., J. Wadsworth, and O. D. Sherby. "Harper-Dorn creep in pure metals." Acta Metallurgica 36, no. 4 (1988): pp.1117-1128.
[28] Mohammed, F. A., Murty, K.L. and Morris, J. W., Jr. In: The John E. Dorn Memorial Symposium. Cleveland, Ohio, ASM(1973).
[29] Ashby, M., Shercliff, H., and Cebon, D., Materials: Engineering, Science, Processing and Design. Butterworth-Heinemann, Oxford. 2013.
[30] Ashby, M. F. and Jones, D. R. H., "Engineering Materials 1: An Introduction to Their Properties and Applications". Oxford: Butterworth Heinemann, 2nd ed., 1996.
[31] Dimmler, G., P. Weinert, and H. Cerjak. "Investigations and analysis on the stationary creep behaviour of 9–12% chromium ferritic martensitic steels." Materials for Advanced Power Engineering 2002 (2002): pp.1539-1550.
[32] Dimmler, G., P. Weinert, and H. Cerjak. "Extrapolation of short-term creep rupture data—The potential risk of over-estimation." International journal of pressure vessels and piping 85, no. 1 (2008): pp.55-62.
[33] Langdon, Terence G. "Creep at low stresses: An evaluation of diffusion creep and Harper-Dorn creep as viable creep mechanisms." Metallurgical and Materials Transactions A 33, no. 2 (2002): pp.249-259.
[34] Yavari, Parviz, and Terence G. Langdon. "An examination of the breakdown in creep by viscous glide in solid solution alloys at high stress levels." Acta Metallurgica 30, no. 12 (1982): pp.2181-2196.
[35] Larson, F. R., Miller, J., 1952, "A time temperature relationship for rupture and creep stress," Trans. ASME. 74, pp. 765–775.
[36] Monkman, F. C. (1956). An empirical relationship between rupture life and minimum creep rate in creep rupture tests. In proc. ASTM (Vol. 56, pp. 91-103).
[37] Maruyama, K., Abe, F., Sato, H., Shimojo, J., Sekido, N.,Yoshimi, K., 2018, "On the physical basis of a Larson-Miller constant of 20," International Journal of Pressure Vessel and Piping,159, pp. 93–100. doi:10.1016/j.ijpvp.2017.11.013.
[38] Onizawa, T., Wakai, T., Ando, M, Aoto, K, 2008, "Effect of V and Nb on precipitation behavior and mechanical properties of high Cr steel," Nuclear Engineering and Design, 238(2), pp. 408-416. doi: 10.1016/j.nucengdes.2006.09.013
[39] Kumar, J. G., Ganesan, V., Laha, K., and Mathew, M. D., 2013, "Time dependent design curves for a high nitrogen grade of 316LN stainless steel for fast reactor applications," *Nuclear Engineering and Design*, 265, pp. 949-956. doi: 10.1016/j.nucengdes.2013.09.035
[40] Haque, M. S., & Stewart, C. M. (2019). Comparative analysis of the sin-hyperbolic and Kachanov–Rabotnov creep-damage models. International Journal of Pressure Vessels and Piping, 171, 1-9.
[41] Kachanov, L. M., 1967, The Theory of Creep, National Lending Library for Science and

Technology, Boston Spa, England, Chaps. IX, X.
[42] Rabotnov, Y. N., 1969, Creep Problems in Structural Members, North Holland, Amsterdam.
[43] Evans, R., and Wilshire, B., 1985, Creep of metal and alloys, Institute of Metals, London.
[44] Prager, M., 1995, Development of the MPC Omega Method for Life Assessment in the Creep Range, Journal of Pressure Vessel Technology, 117(2), pg. 95-103.
[45] Liu, Y., & Murakami, S. (1998). Damage localization of conventional creep damage models and proposition of a new model for creep damage analysis. JSME International journal series A solid mechanics and material engineering, 41(1), 57-65.
[46] Hyde, C. J., Sun, W., Hyde, T. H., Saber, M., & Becker, A. A. (2014). Application of the Liu and Murakami damage model for creep crack growth predictions in power plant steels.
[47] Stewart, C. M., & Gordon, A. P. (2012). Strain and Damage-Based Analytical Methods to Determine the Kachanov–Rabotnov Tertiary Creep-Damage Constants. International Journal of Damage Mechanics, 21(8), 1186-1201.
[48] Haque, M. S., & Stewart, C. M. (2016, July). Modeling the creep deformation, damage, and rupture of Hastelloy X Using MPC omega, theta, and sin-hyperbolic models. In ASME 2016 Pressure Vessels and Piping Conference. American Society of Mechanical Engineers Digital Collection.
[49] Bendick, W., Gabrel, J., Hahn, B., & Vandenberghe, B. (2007). New low alloy heat resistant ferritic steels T/P23 and T/P24 for power plant application. International Journal of Pressure Vessels and Piping, 84(1-2), 13-20.
[50] Pandey, C., Mahapatra, M. M., Kumar, P., & Saini, N. (2018). Some studies on P91 steel and their weldments. Journal of Alloys and Compounds
[51] Guguloth, K., & Roy, N. (2017). Creep deformation behavior of 9Cr1MoVNb (ASME Grade 91) steel. Materials Science and Engineering: A, 680, 388-404.
[52] Panait, C. G., Bendick, W., Fuchsmann, A., Gourgues-Lorenzon, A. F., & Besson, J. (2010). Study of the microstructure of the Grade 91 steel after more than 100,000 h of creep exposure at 600 C. International journal of pressure vessels and piping, 87(6), 326-335.
[53] NIMS- Database for P91 Creep Datasheet 43A, http://smds.nims.go.jp/MSDS/pdf/sheet/C43AJ.pdf, [2018-06-06]
[54] Kimura, K., Kushima, H., & Sawada, K. (2009). Long-term creep deformation property of modified 9Cr–1Mo steel. Materials Science and Engineering: A, 510, 58-63.
[55] Holdsworth, S. R., Askins, M., Baker, A., Gariboldi, E., Holmström, S., Klenk, A., ... & Spigarelli, S. (2008). Factors influencing creep model equation selection. International Journal of Pressure Vessels and Piping, 85(1-2), 80-88
[56] Golan, O., Arbel, A., Eliezer, D., & Moreno, D. (1996). The applicability of Norton's creep power law and its modified version to a single-crystal superalloy type CMSX-2. Materials Science and Engineering: A, 216(1-2), 125-130.
[57] Hug, E., Keller, C., Favergeon, J., & Dawi, K. (2009). Application of the Monkman–Grant law to the creep fracture of nodular cast irons with various matrix compositions and structures. Materials Science and Engineering: A, 518(1-2), 65-75.
[58] Kassner, Michael E. Fundamentals of creep in metals and alloys. Butterworth-Heinemann, 2015.
[59] Phaniraj, C., Choudhary, B. K., Rao, K. B. S., & Raj, B. (2003). Relationship between time to reach Monkman–Grant ductility and rupture life. Scripta Materialia, 48(9), 1313-1318.
[60] Burt, H. & Wilshire, B. Metall and Mat Trans A (2006) 37: 1005. https://doi.org/10.1007/s11661-006-0073-3

[61] Wilshire, B., & Battenbough, A. J. (2007). Creep and creep fracture of polycrystalline copper. Materials science and engineering: a, 443(1-2), 156-166.
[62] Kumar, P., Kassner, M. E., and Langdon, T. G., 2007, "Fifty years of Harper–Dorn creep: a viable creep mechanism or a Californian artifact?."Journal of Materials Science, 42(2), pp. 409-420.
[63] Wilshire, B., & Scharning, P. J. (2007). Long-term creep life prediction for a high chromium steel. Scripta Materialia, 56(8), 701-704.
[64] Wilshire, B., Scharning, P. J., & Hurst, R. (2007). New methodology for long term creep data generation for power plant components. Energy Materials, 2(2), 84-88.
[65] Wilshire, B., & Scharning, P. J. (2008). A new methodology for analysis of creep and creep fracture data for 9–12% chromium steels. International materials reviews, 53(2), 91-104.
[66] Wilshire, B., & Scharning, P. J. (2008). Prediction of long term creep data for forged 1Cr–1Mo–0· 25V steel. Materials science and technology, 24(1), 1-9.
[67] Whittaker, M. T., & Harrison, W. J. (2014). Evolution of Wilshire equations for creep life prediction. Materials at High Temperatures, 31(3), 233-238.
[68] Evans, M. (2015). Constraints Imposed by the Wilshire Methodology on Creep Rupture Data and Procedures for Testing the Validity of Such Constraints: Illustration Using 1Cr-1Mo-0.25 V Steel. Metallurgical and Materials Transactions A, 46(2), 937-947.
[69] Abdallah, Z., Perkins, K., & Williams, S. (2012). Advances in the Wilshire extrapolation technique—Full creep curve representation for the aerospace alloy Titanium 834. Materials Science and Engineering: A, 550, 176-182.
[70] Zhao, Y. R., Yao, H. P., Song, X. L., Jia, J., & Xiang, Z. D. (2017). On the physical models for predicting the long-term creep strengths and lifetimes of modified 9Cr-1Mo steel. Journal of Alloys and Compounds, 726, 1246-1254.
[71] Whittaker, M. T., Evans, M., & Wilshire, B. (2012). Long-term creep data prediction for type 316H stainless steel. Materials Science and Engineering: A, 552, 145-150.
[72] Cedro, V., Garcia, C., & Render, M. (2018). Use of the Wilshire Equations to Correlate and Extrapolate Creep Data of HR6W and Sanicro 25. Materials, 11(9), 1585.
[73] Abdallah, Z., Gray, V., Whittaker, M., & Perkins, K. (2014). A critical analysis of the a conventionally employed creep lifting methods. Materials, 7(5), 3371-3398.
[74] Harrison, W., Whittaker, M., & Williams, S. (2013). Recent advances in creep modelling of the nickel base superalloy, alloy 720Li. Materials, 6(3), 1118-1137.
[75] Evans, M., & Williams, T. (2019). Assessing the capability of the Wilshire equations in predicting uniaxial creep curves: An application to Waspaloy. International Journal of Pressure Vessels and Piping, 172, 153-165.
[76] Haque, M. S. (2015). An improved Sin-hyperbolic constitutive model for creep deformation and damage, Master's Thesis, ETD Collection for University of Texas, El Paso. AAI1591958.
[77] Haque, M. S., and Stewart, C. M., 2016, "Finite Element Analysis of Waspaloy Using Sinh Creep-Damage Constitutive Model under Triaxial Stress State," ASME Journal of Pressure Vessel Technology, 138(3). doi: 10.1115/1.4032704
[78] Haque, M. S., and Stewart, C. M., 2016, "Modeling the Creep Deformation, Damage, and Rupture of Hastelloy X using MPC Omega, Theta, and Sin-Hyperbolic Models," ASME PVP 2016, PVP2016-63029, Vancouver, BC, Canada, July 17-21, 2016.
[79] Haque, M. S., and Stewart, C. M., 2017, "The Stress-Sensitivity, Mesh-Dependence, and Convergence of Continuum Damage Mechanics Models for Creep," ASME Journal of Pressure Vessel Technology, 139(4). doi:10.1115/1.4036142

[80] Giannopoulos, I. P., & Burgoyne, C. J. (2011). Prediction of the long-term behaviour of high modulus fibres using the stepped isostress method (SSM). Journal of materials science, 46(24), 7660-7671.
[81] Tanks, J., Rader, K., Sharp, S., & Sakai, T. (2017). Accelerated creep and creep-rupture testing of transverse unidirectional carbon/epoxy lamina based on the stepped isostress method. Composite Structures, 159, 455-462.
[82] Wheeldon, J. M., & Shingledecker, J. P. (2013). Materials for boilers operating under supercritical steam conditions. In Ultra-Supercritical Coal Power Plants (pp. 81-103). Woodhead Publishing.

VITA

My name is Jaime Aaron Cano. I have earned my Bachelor of Science degree in Mechanical Engineering from the University of Texas at El Paso (UTEP). I graduated with cum laude honors in May 2018. This thesis is submitted as a requirement for the completion of a master's degree in Mechanical Engineering at UTEP as well under the supervision of Dr. Calvin M. Stewart. The current work is a compilation of the work I have done as a research assistant in the Materials at Extremes Research Group (MERG). At MERG, I have conducted research on the creep mechanics of superalloys for Advanced Ultra-Supercritical CO2 power plants. Topics including creep deformation, damage, rupture and creep-fatigue. As well as model, new constitutive model development for predictions of creep deformation using the Wilshire model embedded in the continuum damage mechanics (CDM) framework.

The publications related to this work are:

1) Cano, J.A., and Stewart, C.M, 2019 "Application of the Wilshire Stress-Rupture and Minimum-Creep-Strain-Rate Prediction Models for Alloy P91 in Tube, Plate and Pipe Form." Proceedings of ASME Turbo Expo 2019: Turbomachinery Technical Conference and Exposition, Phoenix, Arizona, USA. June 17-21, 2019, ASME Paper No. GT2019-90625.
2) Cano, J.A., and Stewart, C.M, 2019, "A Continuum Damage Mechanics (CDM) based Wilshire Model for Long-Term Creep Deformation and Damage Prediction" Material Science and Technology. (Manuscript in preparation).

Contact information: Jaime Aaron Cano, institute email: jacano2@miners.utep.edu, personal email: eng.jacano2@gmail.com